Plant Physiology and Biochemistry 232 (2026) 111064

Contents lists available at ScienceDirect

Plant Physiology and Biochemistry

journal homepage: www.elsevier.com/locate/plaphy

Soil compaction impairs cotton growth and photosynthetic performance even under non-limiting water and nutrient conditions

Camila P. Cagna [a,b,*], Cássio A. Tormena [a], Renan Falcioni [a,d], Fabio R. Echer [c], Olanrewaju H. Ologunde [b], Marcio R. Nunes [b], Werner C. Antunes [d]

[a] Agronomy Department, State University of Maringa, Maringa, Parana, Brazil
[b] Soil, Water, and Ecosystem Sciences Department, University of Florida, Gainesville, FL, United States
[c] Agronomy Department, São Paulo Western University, Presidente Prudente, São Paulo, Brazil
[d] Biology Department, State University of Maringa, Maringa, Parana, Brazil

ARTICLE INFO

Keywords:
Soil physical properties
Growth analysis
Photosystem
Thylakoids
Stomatal conductance

ABSTRACT

Soil compaction represents a critical limitation to global agricultural productivity, yet how its direct effects plant physiological processes remain insufficiently understood. This study assessed how increasing levels of soil compaction influence the physiological performance of cotton (*Gossypium hirsutum*) under controlled environmental conditions. Three degrees of compaction (DC) were considered: Control – 75% of the maximum soil bulk density (Bd = 1.52 Mg m^{-3}, non-compacted), DC85 (Bd = 1.66 Mg m^{-3}) and DC95 (Bd = 1.78 Mg m^{-3}) corresponded to intermediate and high compaction levels, representing 85% and 95% of the soil's maximum bulk density, respectively. Increasing compaction significantly reduced plant growth and leaf area. Photosynthesis was suppressed due to stomatal closure, which limited CO_2 diffusion into mesophyll tissue, and was accompanied by decreased photochemical and carboxylation efficiencies. Soil compaction promotes on cotton plants increased thermal energy dissipation, reduced electron transport efficiency between Q_A and Q_B, and altered chloroplast ultrastructure, including the number of chloroplasts and organization of thylakoid lamellae. These changes impaired light harvesting and CO_2 fixation. Additionally, high compaction levels led to increased leaf reflectance and reduced sugar content, indicating compromised source activity, although no direct evidence of end-product feedback inhibition was observed. Overall, soil compaction negatively affected photosynthetic performance at multiple levels, morphological, anatomical, biochemical, and photochemical, culminating in reduced carbon assimilation and biomass accumulation in cotton. These findings highlight the critical role of maintaining adequate soil physical conditions to ensure optimal photosynthetic function and crop performance.

1. Introduction

Agricultural mechanization boosts productivity by enhancing operational efficiency and reducing labor costs, however, the machinery traffic during field operations can lead to soil compaction (Jamali et al., 2021). Compaction alters soil structure resulting in aggregate breakdown and disrupts soil-water and air fluxes, impairing water infiltration and soil aeration as well as increasing soil resistance to root penetration (Colombi and Keller, 2019; Hamza and Anderson, 2005). It is estimated that agricultural machinery has compacted approximately 68 million hectares of arable land, with this situation expected to rise as machinery becomes heavier (Merten and Minella, 2013; Schjonning et al., 2015; Keller and Or, 2022, Keller et al., 2019). Despite mitigation strategies such as conservation agriculture and controlled traffic farming, soil compaction remains a persistent issue with significant negative impacts on agricultural productivity (Anghinoni et al., 2019; Nouri et al., 2019; Keller et al., 2019).

Soil compaction adversely affects cotton production systems due to the crop's sensitivity to soil compaction. Cotton growth and productivity decline markedly with increasing soil compaction (Rivera et al., 2019). In Australia, for example, 66% of cotton farms are affected by compaction, which is primarily caused by the use of agricultural machinery during crop season (CCA, 2020). Pre-planting operation of machinery on wet soil can decrease air-filled-porosity by 30%, changing

This article is part of a special issue entitled: Plant stress responses published in Plant Physiology and Biochemistry.

* Corresponding author. Agronomy Department, State University of Maringa, Maringa, Parana, Brazil.
E-mail address: camilacagna@ufl.edu (C.P. Cagna).

https://doi.org/10.1016/j.plaphy.2026.111064
Received 8 June 2025; Received in revised form 22 December 2025; Accepted 19 January 2026
Available online 30 January 2026

soil physical processes and reducing cotton yields (McGarry, 1990). Additionally, compacted soils may require up to three times more irrigation to maintain fiber yields, thereby reducing water use efficiency and raising production costs (McGarry, 1995).

Cotton is among the most important crops grown in Brazil and worldwide. Within the Brazilian savanna biome, cotton is typically grown in a short rotation with soybeans, often without the inclusion of cover crops. The intensive use of heavy machinery for cotton production has led to severe soil compaction levels, with a noticeable decline in crop yields by the third cropping cycle (Shaheb et al., 2021). Consequently, farmers have used mechanical practices (e.g., subsoiling) every 3–5 years to mitigate soil compaction. Preliminary results have shown that these limiting changes within the soil can simultaneously affect various physiological processes (Huntenburg et al., 2021; Mariotti et al., 2020). For instance, increased soil mechanical resistance delays radicle penetration during seedling establishment (Jamali et al., 2021), reduces water infiltration, and heightens seedling mortality caused by pathogens (e.g., Rhizoctonia), thereby reducing plant establishment. Severe compaction combines physical soil changes with physiological dysfunctions, reducing photosynthetic rates due to smaller stomatal openings and restricted CO_2 diffusion to mesophyll (Wieniarska et al., 1987; Masle and Passioura, 1987). Collectively, these factors have great potential to reduce crop growth and yield.

Despite cotton is a crop of significant economic importance, yet the effects of soil compaction on its growth remain underexplored, especially in regions where soils are susceptible to compaction (Silva et al., 2024). Although previous research has independently investigated soil physical properties and crop yield (Anghinoni et al., 2019; Hamza and Anderson, 2005), only a few assessments have explored how soil compaction collectively influences both soil properties and plant physiological processes, which are critical to crop productivity. Understanding the mechanisms by which soil compaction affects cotton growth is essential for developing effective strategies to mitigate its negative impact within this crop production system. In particular, such insights would advance our knowledge of how compaction limits photosynthesis and the overall growth of cotton. Therefore, this study aims to quantify the direct impact of soil compaction on the physiological processes of cotton plants including root and shoot growth, photosynthetic efficiency, anatomical and ultrastructural changes, leaf pigments, spectral data, and metabolic activity.

2. Material and methods

2.1. Plant material and experimental design

The experiment was conducted in a greenhouse at the Department of Agronomy, State University of Maringa, Brazil. The soil used was a sandy Ferrasol (111 g kg^{-1} clay, 16 g kg^{-1} silt, and 872 g kg^{-1} sand). Cotton plants (cultivar FM 974GLT, BASF/FiberMax) were grown under a completely randomized design with three treatments and five replicates. Treatments consisted of: (i) Control – cotton grown in soil compacted to 75% degree of compaction (DC, proctor method) considered non-compacted with a soil bulk density (BD of 1.52 Mg m^{-3}); (ii) DC85 – cotton grown in soil with an 85% degree of compaction (intermediate compaction – BD of 1.66 Mg m^{-3}); and DC95 – cotton grown in soil with a 95% degree of compaction (high compaction – BD of 1.78 Mg m^{-3}). Experimental unit consisted of a PVC cylinder (25 cm diameter and 25 cm height), filled with soil and one plant per cylinder. The base of each cylinder was wrapped with nonwoven fabric.

Five cotton seeds were sown per cylinder at a 3 cm depth and thinned to one plant 10 days after emergence. To maintain adequate soil moisture and nutrient availability, each experimental unit received daily irrigation (400 mL of water) and 100 mL of Hoagland nutrient solution every two days. Irrigation was applied directly to the tray in which the cylinders were placed, allowing water to rise into the soil by capillarity. Before establishing the experiment, a one-week preliminary test was conducted to validate the irrigation strategy. The same cylinders and soil compaction treatments were used, and two tensiometers were installed at 7 cm and 20 cm depth in each cylinder. Soil water potential remained consistently close to field capacity and never approached saturation, indicating that part of the pore space remained air-filled even under compacted conditions. This confirmed that the capillary irrigation system maintained stable moisture levels without compromising soil aeration or oxygen availability to the roots. In addition, air-filled porosity was monitored throughout the experiment. Across all treatments, values remained at or above the minimum threshold of 0.10 m^3 m^{-3} recommended by Grable and Siemer, (1968) and Pragg et al. (2024), with measured values of 0.15 m^3 m^{-3} for the Control, 0.10 m^3 m^{-3} for DC85, and 0.10 m^3 m^{-3} for DC95.

2.2. Soil physical properties

At the end of the experiment, undisturbed soil cores (5 cm height × 7.5 cm diameter) were collected from each treatment (n = 15). To avoid evaporative losses, immediately after collection, samples were wrapped in aluminum foil and refrigerated at 5 °C for subsequent analysis.

Soil cores were saturated by capillary rise for 24 h. Soil water retention was determined at matric potentials of −3, −6, and −10 kPa using a tension table, following Reynolds et al. (2002). Water contents at −10 kPa and −1500 kPa were interpreted as field capacity (FC) and permanent wilting point (PWP), respectively (Savage et al., 1996). For potentials of −1000 and −1500 kPa, water content was measured using a WP4-C dewpoint psychrometer on sieved (<2 mm) samples. After equilibration at the final matric potential, samples were oven-dried at 105 °C for 24 h to quantify gravimetric water content.

Water storage capacity was calculated as the ratio of FC to total porosity (TP), and air storage capacity as the ratio between air-filled porosity (AC) and TP, based on Reynolds et al. (2002). Air-filled porosity was computed by subtracting water content at −10 kPa from the saturated water content.

Plant available water (PAW) was calculated as the difference between soil water content at field capacity and permanent wilting point, as described by De Jong Van Lier et al. (2023). PAW was expressed in millimeters (mm), calculated by multiplying the water content difference (FC – PWP) by the soil layer thickness (z, mm):

$$PAW = (FC - PWP)*z \quad (1)$$

Critical water content associated with a penetration resistance (PR) of 2 MPa (θ_{2MPa}) was determined by progressively air-drying the cores at room temperature. PR was measured repeatedly (sever readings per core) using a bench penetrometer with a 4 mm diameter cone and 30° semi-angle at a constant speed of 0.01 m min^{-1}. PR data were recorded simultaneously with sample weights to relate PR to volumetric water content (θ). An exponential model was fitted to describe the PR(θ) relationship:

$$PR = a\theta^b \quad (2)$$

$$\theta_{2\ MPa} = \frac{2\ MPa}{a^{1/b}} \quad (3)$$

where a and b are model parameters. A PR threshold of 2 MPa was considered critical, as suggested by Blainski et al. (2008).

Soil air permeability (Kair) was assessed on samples equilibrated at −10 kPa using a constant head permeameter, as described by Ball and Schjonning (2002). Airflow was regulated by a mass flow controller, and differential pressure was monitored using a manometer. Kair (μm^2) was calculated as:

$$K_{air} = \left[\frac{Q\eta}{A_s}\right] x \left[\frac{z}{P}\right] \quad (4)$$

where Q is airflow (m^3 s^{-1}), η is air viscosity at 20 °C (1.84 × 10^{-5} N s

m^{-2}), A_s is the sample cross-sectional area (m^2), z is sample height (m), and P is the pressure differential (Pa).

Bulk density (Bd) was obtained as the ratio between dry soil mass to the core volume (Blake and Hartge, 1986). Total porosity (TP) was estimated as (equation (5)):

$$TP = 1 - \frac{Bd}{Pd} \quad (5)$$

where particle density (Pd) was assumed to be 2.65 Mg m^{-3}(Flint and Flint, 2002).

Pore size classes, macropores, mesopores, and micropores (Mi), were estimated from soil water contents at matric potentials of −3 and −10 kPa, as described by Lima et al. (2022). Pore diameter thresholds were defined according to Koorevaar et al. (1983), considering macropores as >100 μm, mesopores as 30–100 μm, and micropores as <30 μm. The corresponding volumes for each pore class were calculated using the equations below.

$$Ma = TP - \theta_{3\ kPa} \quad (6)$$

$$Me = \theta_{3\ kPa} - \theta_{10\ kPa} \quad (7)$$

$$Mi = \theta_{10\ kPa} \quad (8)$$

where θ_3 kPa and θ_{10} kPa are the soil water content at matric potentials of −3 and −10 kPa, respectively.

2.3. Plant growth analyses

A destructive growth analysis was conducted 67 days after seedling emergence, following Hoffmann and Poorter (2002) and Falcioni et al. (2018). Roots, stems, and leaves were separated and oven-dried at 70 °C for 72 h using a forced-air oven to determine their dry mass. Leaf area was quantified with an LI-3100C leaf area meter (LI-COR Inc., Nebraska, USA). Based on these measurements, total biomass, leaf mass fraction (LMF), stem mass fraction (SMF), root mass fraction (RMF), specific leaf area (SLA), relative growth rate (RGR), and unit leaf rate (ULR) were calculated.

2.4. Nutrient measurements

Dried cotton leaves were ground to a fine powder using a Wiley mill with stainless steel blades to obtain homogeneous samples. One gram of material (dry weight) was used for nutrient analysis. Nitrogen (N) content was quantified following complete digestion in concentrated H_2SO_4, with subsequent distillation using the micro-Kjeldahl method. Total phosphorus (P), potassium (K), calcium (Ca), magnesium (Mg), copper (Cu), iron (Fe), manganese (Mn), and zinc (Zn) were determined after digestion in a 4:1 nitric–perchloric acid solution. Concentrations of Ca, Mg, Cu, Fe, Mn, and Zn were measured using a microwave plasma–atomic emission spectrometer (MP-AES; Agilent®). Potassium and phosphorus contents were quantified using a flame photometry and by colorimetric analysis based on metavanadate complex formation, respectively. All procedures followed the protocols outlined by Malavolta et al. (1997).

2.5. Hyperspectral optical leaf properties

Leaf reflectance (R) and transmittance (T) were measured using a FieldSpec® 3 spectroradiometer (Analytical Spectral Devices, ASD Inc., Longmont, CO, USA) coupled to an ASD Contact PlantProbe® featuring a 10 mm diameter sensor. The instrument contained 512 silicon photodiodes, enabling spectral measurements from 350 to 2500 nm. A PlantProbe® leaf clip (ASD Inc.) was used to minimize atmospheric interference during data acquisition. Calibration was performed using Spectralon® white reference panels (Labsphere Inc., Longmont, CO, USA), following Falcioni et al. (2023a).

A high-intensity light source from the PlantProbe® was applied to the adaxial leaf surface, while transmittance through the abaxial surface was recorded using a second probe with the light source turned off. Reflectance and transmittance spectra were collected simultaneously across all wavelength. Leaf absorbance (A) was calculated as A = 1 − (R + T). Spectral data from 350 to 1100 nm were integrated with pigment content (extracted using acetone), as described by Falcioni et al. (2017).

2.6. Photosynthetic pigments

A fully expanded but still young leaf segment (1 cm^2) was incubated in darkness for 16–20 h in an 80:20 (v/v) acetone-water solution for pigment extraction. Spectral absorbance of the extracted pigments was measured from 350 to 1100 nm using a UV–VIS–NIR spectrophotometer (UV-3600 Plus, Shimadzu Inc., Tokyo, Japan). Absorbance at 470, 647, and 663 nm was used to calculate chlorophyll and carotenoid concentrations on a leaf area basis, following Lichtenthaler (1987). To express pigment content per dry weight (DW), an adjacent portion of the same leaf was collected, oven-dried, and weighed.

2.7. Gas exchange measurements

2.7.1. Light curves with multiphase Flash™ fluorometer

Gas exchange was measured on fully expanded yet physiologically active leaves (typically the 5th or 6th from the shoot apex) at 56 days after seedling emergence. A portable infrared gas analyzer (LI−6800, LI−COR Inc., Lincoln, NE, USA), equipped with a Multiphase Flash™ Fluorometer (LI−6800−01) was used to quantify net CO_2 assimilation rate (A), intercellular CO_2 concentration (C_i), stomatal conductance (g_s), and transpiration rate (E). Photosynthetic light-response curves were generated using a built-in light source providing photosynthetically active radiation (PAR) at the following intensities: 2500, 2000, 1800, 1500, 1200, 1000, 800, 600, 400, 300, 200, 150, 100, 75, 50, 25, and 0 μmol m^{-2} s^{-1}.

Measurements were conducted under controlled chamber conditions: 400 μmol mol^{-1} CO_2, 60% relative humidity, 90:10 red:blue light ratio, 25 °C chamber temperature, 700 μmol s^{-1} airflow, and 10,000 rpm fan speed. Fluorescence parameters under light-adapted conditions were recorded concurrently, and dark-adapted fluorescence was measured pre-dawn on the same leaf sample.

Photosynthetic parameters including apparent quantum yield (α) [(μmol CO_2 m^{-2} s^{-1})/(μmol photons m^{-2} s^{-1})], light compensation point (LCP), light saturation point (LSP), maximum net photosynthetic rate (A_{MAX}), and dark respiration (Rd) were derived by fitting the light response curve using the non-rectangular hyperbola model:

$$\left[PN = \frac{[\phi(I0) \times I \times Pg_{MAX}]}{[\phi(I0)^2 \times I^2 + Pg_{MAX}{}^2]^{0.5}} - Rd\right] \quad (9)$$

where PN is net photosynthesis rate [μmol (CO_2) m^{-2} s^{-1}]; $\phi_{(I0)}$ is quantum yield at zero light [μmol (CO_2) $mmol^{-1}$ (photons)]; I is the photosynthetic photon flux density [μmol (photons) m^{-2} s^{-1}]; Pg_{MAX} is the maximum gross photosynthesis rate [μmol (CO_2) m^{-2} s^{-1}]; and Rd is the dark respiration rate [μmol (CO_2) m^{-2} s^{-1}].

Intrinsic water use efficiency (*i*WUE) was calculated as A/g_s [(μmol CO_2 m^{-2} s^{-1})/(mol H_2O m^{-2} s^{-1})] to evaluate the physiological efficiency of CO_2 uptake relative to stomatal conductance. Adjustments for leaf structural traits were incorporated based on specific leaf area (SLA).

2.7.2. $A-C_i$ curves with multiphase Flash™ fluorometer

Photosynthetic CO_2 response curves (A–C_i) were constructed under controlled conditions while simultaneously chlorophyll fluorescence. Leaves were exposing to a sequence of reference CO_2 concentrations in the sample chamber (400, 300, 200, 100, 50, 25, 400, 600, 800, 1000, 1200, 1400, 1600, 1800, and 2000 μmol mol^{-1}), under a constant

photosynthetic photon flux density of 1200 μmol m^{-2} s^{-1} (PAR) provided by the instrument's integrated light source. Each CO_2 step was applied for 50–70 s under a red:blue light ratio of 90:10.

Measurements were performed using a LI-6800 IRGA system (LI-COR Inc., Lincoln, NE, USA) with the following parameters: 60% relative humidity in the sample chamber, flow rate of 700 μmol s^{-1} with pressure differential (ΔP) set at 0.1, vapor pressure deficit (VPD) automatically regulated, fan speed of 10,000 rpm, and a chamber temperature of 25 °C.

Carboxylation parameters were estimated from the response curves, including the maximum rate of Rubisco carboxylation (VC_{MAX}; μmol CO_2 m^{-2} s^{-1}), maximum electron transport rate (J_{MAX}; μmol photons m^{-2} s^{-1}), and the maximum rate of triose phosphate utilization (TPU; μmol CO_2 m^{-2} s^{-1}). Parameter estimation was carried out using the 'PCE_Calculator_Curve_Fitting_Model 2.0′ script developed by Sharkey (2016) and published in "Plant, Cell and Environment". The model was adjusted to standard environmental constants: leaf temperature of 25 °C, atmospheric pressure of 101 kPa, and O_2 concentration of 21 kPa, as recommended by Sharkey (2016).

2.7.3. Daily photosynthetic measurements

Diurnal gas-exchange were monitored hourly from 5:00 AM to 7:00 PM using an infrared gas analyzer (LI-6800, LI-COR Inc., Lincoln, NE, USA) equipped with a Multiphase Flash™ Fluorometer (LI-6800-01). The system was configured to assess net photosynthetic rate (A), intercellular CO_2 concentration (C_i), stomatal conductance (g_s), and transpiration rate (E). Photosynthetically active radiation (PAR) was fixed at 1000 μmol m^{-2} s^{-1} during the measurements, except for the first and last readings, which were performed in the darkness.

Environmental conditions inside the chamber were strictly controlled: 90:10 red:blue light ratio, 400 μmol mol^{-1} CO_2, 60% relative humidity, 700 μmol s^{-1} airflow, 10,000 rpm fan speed, and a constante temperature of 25 °C. The experimental setup followed the protocols described previously in Sections 2.8.1 and 2.8.2.

2.7.4. Collection of fluorescence OJIP data

Chlorophyll *a* fluorescence induction kinetics (OJIP) were measured using the LI-6800 gas exchange system (LI-COR Inc., Lincoln, NE, USA). Leaves were dark-acclimated overnight in a humid environment to ensure full relaxation of the photosystems. Fluorescence induction curves were recorded under the standardized conditions: chamber area of 6 cm^2, 75% relative humidity, 400 ppm CO_2 concentration, 10,000 rpm fan speed, and a saturating light pulse (625 nm) applied at 15,000 μmol m^{-2} s^{-1} for 1 s. Measurements were acquired in dark-adapted mode at 500 Hz, with a flash mode output of 250 kHz, synchronized to the induction curve acquisition mode (Falcioni et al., 2023a).

Fluorescence was measured at multiple time intervals (~20 μs, 50 μs, 100 μs, 300 μs, 2 ms, and 30 ms), allowing for the calculation of JIP-test parameters over a time course from 20 μs to 1 s (Fm_{t0}–Fm_{tf}). Data were normalized as variable fluorescence (ΔVt), where t0 denotes initial fluorescence and tf represents the maximum fluorescence at the end of the pulse. Differences across phases of the OJIP transient were analyzed using green leaves under white-light reference, following the protocol of Strasser et al. (2000). Characteristic bands, L-band (~150 μs), K-band (~300 μs), J-band (~2 ms), I-band (~10 ms), and H-band (~40 ms), were computed, generating high-resolution fluorescence curves with 925 data points (Falcioni et al., 2023a).

Each bands reflects distinct energy transfer steps within the photosynthetic electron transport chain, involving components such as plastoquinones, cytochrome b_6f complex, plastocyanin, and ferredoxin. JIP-test parameters were calculated using Biolyzer v4.0® software (Laboratory of Bioenergetics, University of Geneva, Switzerland), following Strasser et al. (2000). Energy flux models at the reaction center and cross-section level (RC-CS) were visualized in CorelDraw (2020)® (Corel Corp., Ottawa, ON, Canada), based on the conceptual framework proposed by Sitko et al. (2017).

2.7.5. Fluorescence measurements

Fluorescence measurements were conducted with the LI-6800 system (LI-COR Inc., Lincoln, NE, USA) equipped with the LI-6800-01 Multiphase Flash Fluorometer. Plants were dark-acclimated for 12 h to allow stabilization of initial (Fo) and maximal (Fm) fluorescence. Variable fluorescence (Fv) was calculated as the difference between Fm and Fo, and the Fv/Fm ratio was used to assess the maximum quantum efficiency of photosystem II (PSII) in dark-adapted leaves.

Fluorescence parameters in light-adapted leaves were also obtained to evaluate photosynthetic light responses. The multiphase flash protocol included a saturating pulse of 15,000 μmol m^{-2} s^{-1}, modulated at 5 kHz (dark) and 50 kHz (light), ensuring high signal-to-noise ratio. Maximum fluorescence under illumination (Fm') was recorded at 250 kHz. Emission was detected at wavelengths above 700 nm.

Using LI-COR's software interface synchronized with gas exchange data, several photosynthetic efficiency indicators were calculated following Baker et al. (2007), including effective PSII quantum yield (Fv'/Fm′), actual PSII efficiency (ΦPSII), CO_2-assimilative PSII efficiency (ΦCO_2), electron transport rate (ETR), non-photochemical quenching (NPQ), photochemical quenching (qP), and non-photochemical quenching coefficient (qN).

2.8. Microscopy sample preparation and analyses

2.8.1. Sample preparation

Leaf samples (1–2 mm^2), collected from the same leaves used for gas exchange measurements, were processed for ultrastructural analysis via optical (OM), scanning electron (SEM), and transmission electron microscopy (TEM). Tissues were fixed in a modified Karnovsky solution (Karnovsky, 1965), consisting of 2.5% glutaraldehyde and 2% paraformaldehyde in 0.05 M cacodylate buffer (pH 7.2). Post-fixation was performed for 6 h in the same buffer containing 1% osmium tetroxide and 1.6% potassium ferrocyanide.

After fixation, samples were incubated overnight in 0.5% uranyl acetate to improve image contrast. Dehydration was carried out using a graded acetone series (30%, 50%, 70%, 80%, 90%, and 100%), followed by three final rinses in absolute acetone. A subset of the material was reserved for SEM, while the remaining tissue was embedded and polymerized in Spurr's low-viscosity epoxy resin. Semi-thin (1 μm) and ultrathin (70 nm) sections were obtained using an ultramicrotome (MTX Powertome X, Boeckeler Instruments RCM Products, Egham, UK) equipped with glass and diamond knives. All reagents were certified for electron microscopy and obtained from Sigma (St. Louis, MO, USA) or Electron Microscopy Sciences (Hatfield, PA, USA).

2.8.2. Optical microscopy

For optical microscopy, semi-thin leaf sections (1 μm) were stained with 1% toluidine blue in borax buffer and heated for 5 s at 70 °C. Observations were conducted using a Leica ICC50 light microscope (Leica Microsystems, Wetzlar, Germany). Evaluated anatomical parameters included total leaf thickness, thickness of palisade and spongy mesophyll, and epidermal thickness on both adaxial and abaxial surfaces. The ratio between spongy and palisade mesophyll was also determined. Morphometric data were obtained using ImageJ software, and contrast enhancement and color-based quantification were carried out using Image-Pro Plus®.

2.8.3. Scanning electron microscopy

Leaf samples were subjected to critical point drying (CPD) using a CPD-030 apparatus (Bal-Tec AG, Balzers, Liechtenstein, Germany) for scanning electron microscopy (SEM) preparation. After drying, samples were affixed to aluminum stubs and sputter-coated with a thin layer of gold (50 mA for 150 s) using a MED010 Balzer evaporator (Bal-Tec AG, Balzers, Liechtenstein, Germany).

Imaging was performed with a Quanta 250 SEM (FEI Company, Oregon, USA) operated at an accelerating voltage of 20 kV. Digital

micrographs were acquired using the built-in FEI imaging software. This protocol enabled detailed examination of stomatal density on both adaxial and abaxial leaf surfaces, as well as morphological characterization of trichomes. Quantitative and qualitative analyses were conducted using Image-Pro Plus® software.

2.8.4. Transmission electron microscopy

Ultrathin sections (70 nm) were collected on 300-mesh copper grids and stained sequentially with 3% uranyl acetate for 30 min and lead citrate for 10 min, following the protocol described by Reynolds (1963). Samples were examined using a JEOL JEM-1400 transmission electron microscope (Leica Microsystems Inc., Illinois, USA) operating at 80 kV and equipped with a digital imaging system. Ultrastructural components, such as chloroplasts, thylakoid membranes, mitochondria, vacuoles, cytoplasm, and plastoglobuli, were evaluated through both qualitative and quantitative analyses using Image-Pro Plus® software.

2.9. Sugar and starch extraction and quantification

Soluble sugars and starch were extracted from lyophilized leaf tissue following the method described by Daloso et al. (2015). Briefly, 10 mg of dried tissue was incubated with 1000 μL of pure methanol at 70 °C for 1 h. After incubation, samples were centrifuged at 14,000 g for 10 min. From the supernatant, 700 μL was transferred to a new tube, and 400 μL of deionized water and 500 μL of chloroform ($CHCl_3$) were added. The mixture was vortexed and centrifuged again to separate phases, and 1000 μL of the polar phase was collected and evaporated in a speed vacuum concentrator.

The remaining pellet from methanol extraction was washed three times with 80% ethanol and used for starch determination after solubilization in hot potassium hydroxide (KOH), as described by Trethewey et al. (1998). Concentrations of glucose, fructose, sucrose, and starch were determined using enzymatic assays coupled to NADH production, with absorbance read at 340 nm. Quantification of all metabolites was based on standard curves generated from known concentrations of each pure compound on the same 96-well plate.

2.10. Statistical analyses

The homogeneity of variances for all variables was assessed using Bartlett's test (Zar, 2010). Quantitative data were subjected to one-way analysis of variance (ANOVA), and results are expressed as mean ± standard error (SE). Differences among treatments were considered statistically significant at $p < 0.05$, as determined by Duncan's multiple range test. When applicable, Pearson's correlation analysis was conducted to evaluate linear relationships between variables.

Additionally, principal component analysis (PCA) was employed to reduce the dimensionality of the dataset and to improve the robustness of statistical inferences for interrelated variables, as recommended by Jolliffe (2002). PCA was applied specifically to interpret patterns in total plant dry matter accumulation under varying levels of soil compaction. The first two principal components were retained and visualized in two-dimensional plots. Clustering significance was set at $p < 0.05$. All statistical procedures were carried out using SAS® software.

3. Results

3.1. Soil physical properties

Increasing compaction levels degraded soil physical properties (Table 1). The DC95 treatment showed 14% higher Bd, 76% higher RP_{FC}, 57% higher $\theta_{2\ MPa}$, 10% higher micro, and 30% greater FC/TP compared to the control. In contrast, TP, macro, AC/TP, and K_{air} were reduced by 21%, 75%, 30%, and 82%, respectively, in DC95. The DC85 treatment presented intermediate values, except for mesoporosity, which was higher in this treatment (Table 1).

Table 1
Soil physical properties under distinct degree of compaction (DC) 75% (control), 85% (DC85), 95% (DC95). Different letters under the bars indicate significant differences between soil compaction conditions, as determined by Duncan's test ($p<0.05$). (n = 5 ± SE).

	Control	DC85	DC95
Bd (Mg m^{-3})	1.52 ± 0.01 a	1.66 ± 0.01 b	1.78 ± 0.00 c
TP ($m^3\ m^{-3}$)	0.42 ± 0.01 a	0.37 ± 0.00 b	0.33 ± 0.00 c
Macro ($m^3\ m^{-3}$)	0.16 ± 0.01 a	0.07 ± 0.01 b	0.04 ± 0.00 c
Meso ($m^3\ m^{-3}$)	0.08 ± 0.00 c	0.11 ± 0.00 a	0.09 ± 0.00 b
Micro ($m^3\ m^{-3}$)	0.18 ± 0.00 b	0.19 ± 0.00 ab	0.20 ± 0.00 a
FC ($m^3\ m^{-3}$)	0.22 ± 0.00 b	0.24 ± 0.00 a	0.24 ± 0.00 a
PWP ($m^3\ m^{-3}$)	0.06 ± 0.00 a	0.07 ± 0.00 a	0.06 ± 0.00 a
PAW (mm)	16.00 ± 0.10 b	18.00 ± 0.01 a	18.00 ± 0.10 a
FC/TP	0.52 ± 0.01 c	0.66 ± 0.01 b	0.74 ± 0.01 a
AC ($m^3\ m^{-3}$)	0.20 ± 0.01 a	0.15 ± 0.00 a	0.11 ± 0.00 a
AC/TP	0.47 ± 0.01 a	0.42 ± 0.01 b	0.33 ± 0.01 c
K_{air} μm^{-2}	7.16 ± 0.75 a	2.40 ± 0.07 b	1.29 ± 0.16 b
$\Theta_{2\ MPa}$ ($m^3\ m^{-3}$)	0.08 ± 0.01 c	0.13 ± 0.00 b	0.19 ± 0.01 a
RP_{FC} (MPa)	0.44 ± 0.11 c	1.07 ± 0.03 b	1.90 ± 0.18 a

Bulk density – Bd, total porosity – TP, macroporosity – Macro, mesoporosity – Meso, microporosity – Micro, field capacity – FC, permanent wilting point – PWP, air capacity – AC, water storage capacity – FC/TP, air storage capacity – AC/TP, air permeability – K_{air}, critical humidity – $\theta_{2\ MPa}$ and penetration resistance in field capacity – RP_{FC}.

3.2. Growth parameters

Compared to the control, plants in DC85 and DC95 had lower length and volume of roots, total dry plant mass, length and diameter of stem, number of leaves, and dry mass and area of leaf (Fig. 1). Rates of leaf expansion and daily accumulated transpiration were lower in DC85 and DC95 than in the control (Fig. 2A and B). Soil compaction decreased plant phylocronic rhythm (the interval of emission and the emergence of sequential leaves) and leaf area, which led to a lower number and dry mass of leaves (Fig. 1E–G). In addition, nutritional analysis showed that macro- and micro-nutrient uptake was not affected by compaction (Table S1), except for copper. Besides total biomass and root biomass, compaction also changed biomass partitioning to root, stem, and leaves of cotton. As root growth was greatly harmed, RMF was reduced by around 35% in DC85 and DC95 (Fig. 2C). Similarly, SMF, LMF, and LAR increased by 40%, 33%, and 37% in the DC85 and DC95 treatments compared to the control (Fig. 2D–F), while URL decreased by 53% in the compacted treatments relative to the control (Fig. 2H).

3.3. Diurnal gas exchange

Over a three-day period, diurnal fluctuations in net photosynthetic rates were observed across treatments by evaluating four key physiological parameters: g_s, A, C_i, and E (Fig. 3 and S1). The DC95 consistently had lower g_s throughout the three days of analysis, with a peak of 0.46 mol $m^{-2}\ s^{-1}$ at 12:00 p.m. (60% lower than the control treatment; Fig. 3). Additionally, DC95 had lower A, reaching a maximum of 19.32 μmol CO_2 $m^{-2}\ s^{-1}$ at 12:00 p.m. (23% lower than the Control) and a minimum of −2.08 μmol CO_2 $m^{-2}\ s^{-1}$ recorded at 6:00 a.m. (dark) (Fig. S1) The trend of E was similar to g_s having lower values in DC95 treatment compared to control, with a maximum of 0.0061 mol $m^{-2}\ s^{-1}$ (39% lower than the Control) and a minimum of 0.0005 mol $m^{-2}\ s^{-1}$ (Fig. S1).

Besides reduced g_s values, DC85 and DC95 had a higher standard error for g_s, which is associated with stomatal patchiness as compared to the control. This patchiness is due to the presence of both open and closed stomata simultaneously (Fig. S2). The stomatal aperture affects both CO_2 influx from surroundings to the stomatal cavity and transpiration rate from leaf to atmosphere, as a result, iWUE doubled in the DC85 and DC95 treatments compared to the control (Fig. S2).

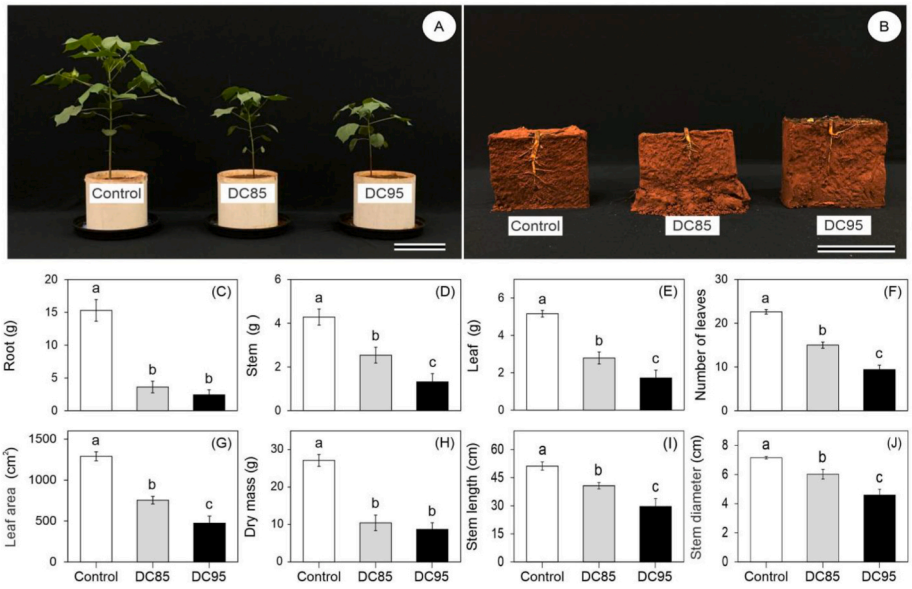

Fig. 1. Cotton plants grown under distinct degree of soil compaction (DC) 75% (control), 85% (DC85), 95% (DC95). From left to right: **(A)** cotton plants after 60 days of the beginning of the experiment and **(B)** soil profile highlighting root development of cotton cultivated after 60 days of the beginning of the treatments under degree compaction of 75%, 85%, and 95% **(C)** root dry matter. **(D)** stem dry matter. **(E)** leaf dry matter. **(F)** number of leaves. **(G)** leaf area. **(H)** total dry mass. **(I)** stem length. **(J)** stem diameter. Different letters above the bars indicate significant statistical differences between treatments under different compaction conditions as determined by Duncan's test ($p<0.05$). (n = 5 ± SE).

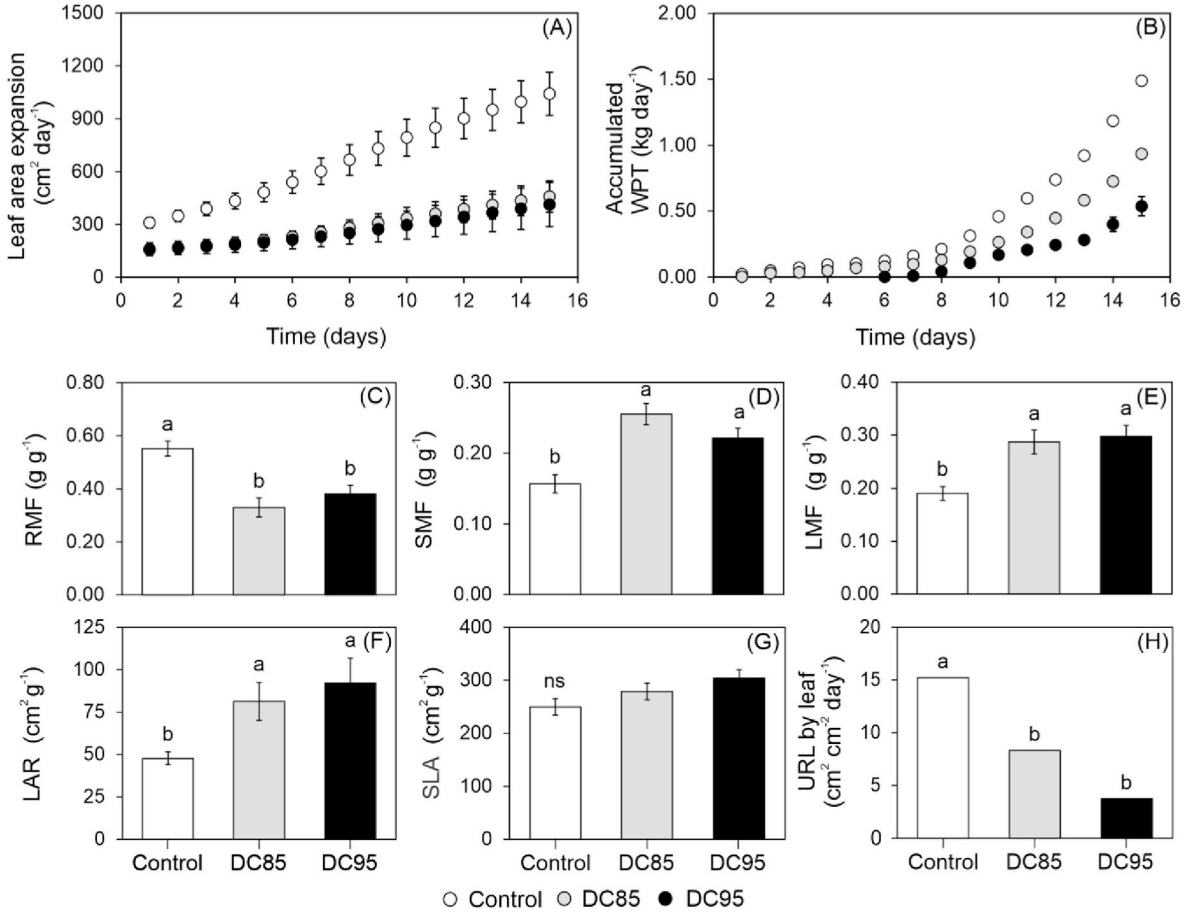

Fig. 2. Cotton plants grown under distinct degree of soil compaction (DC) 75% (control), 85% (DC85), 95% (DC95). **(A)** Leaf area expansion rate. **(B)** Accumulated whole plant transpiration (WPT). **(C)** root mass fraction (RMF). **(D)** stem mass fraction (SMF). **(E)** leaf mass fraction (LMF). **(F)** leaf area ratio (LAR). **(G)** specific leaf area (SLA). **(H)** unit leaf rate (ULR). Different letters over the bars indicate significant statistical differences between plants grown under different compaction conditions, as determined by Duncan's test ($p<0.05$). (n = 5 ± SE).

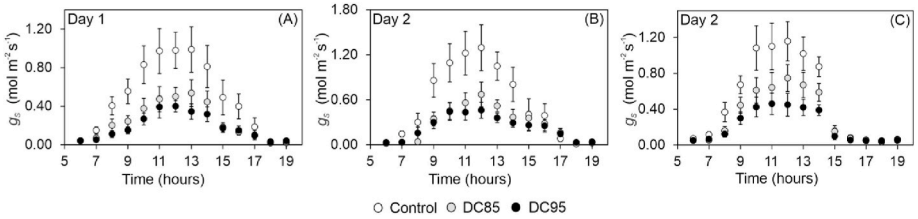

Fig. 3. Daily curves of stomatal conductance (g mol H_2O m^{-2} s^{-1}) between 6 and 19 h were evaluated over three days for cotton plants grown under distinct degree of compaction (DC) 75% (control), 85% (DC85), 95% (DC95). Mean ± SE. (n = 5).

3.4. Leaf pigment content and optical properties

Compared to the control, DC95 and DC85 had plants with lower contents of Chl *a*, Chl *b*, and Chl *a*+*b*, based on leaf area (Fig. 4D–F), Chl *a*/Chl *b* ratio (Fig. 4H), and carotenoids (Car) (Fig. 3H). DC95 had higher reflectance indices (Fig. 4A and S3A) and lower transmittance (Fig. 4B and S3B) and leaf absorbance indices (Fig. 4C and S3C).

3.5. Leaf structure and cellular organization

Microscopy and anatomical analyses of cotton leaves exposed to different levels of soil compaction (Fig. 5A–J) revealed that under the highest compaction condition (DC95), the leaves exhibited greater total thickness (approximately 267 μm; Fig. 5J), representing a 15% increase compared to the control treatment. Particularly spongy parenchyma was thicker under compaction (DC95) while palisade parenchyma showed minor variations with no parallelism to compaction level (Fig. 5J–L). As a result, the spongy-to-palisade parenchyma ratio increased under compaction, with a higher ratio observed in DC95. Abaxial epidermal thickness different among treatments, decreasing in DC95 compared to the control (Fig. 5M and N).

3.6. Morphological analyses of adaxial leaf surfaces

Morphological changes of adaxial epidermis evaluated by scanning electron microscopy (SEM) revealed an increase in the pavement cell area, with an increase in stomatal density between the Control and DC95 (Fig. S4A–I). Additionally, DC85 and DC95 had greater rugosity in the cell surface compared to the Control (Fig. S4A–I). There was also a reduction in guard cell length (Fig. S4K) but an increase in guard cell width at higher compaction levels (Fig. S4L). Notwithstanding the length and width of the stomatal pore were not quantitatively evaluated by this technique (just qualitative), therefore, we consider g_s (stomatal conductance to water vapor) as a better proxy of stomatal aperture.

3.7. Integrated photochemical, carboxylative and fluorescence measurements

Soil compaction reduced the photosynthetic efficiency of cotton plants (Figs. 6–7; Tables 2 and 3). The LSP was reduced by 21.7% and 26.4% in the DC85 and DC95 treatments, respectively, compared to the control, indicating impaired photosynthesis under high irradiance (Fig. 6A). Pg_{MAX} and A_{MAX} were significantly lower in DC85 and DC95, suggesting limitations in CO_2 fixation due to biochemical and diffusional

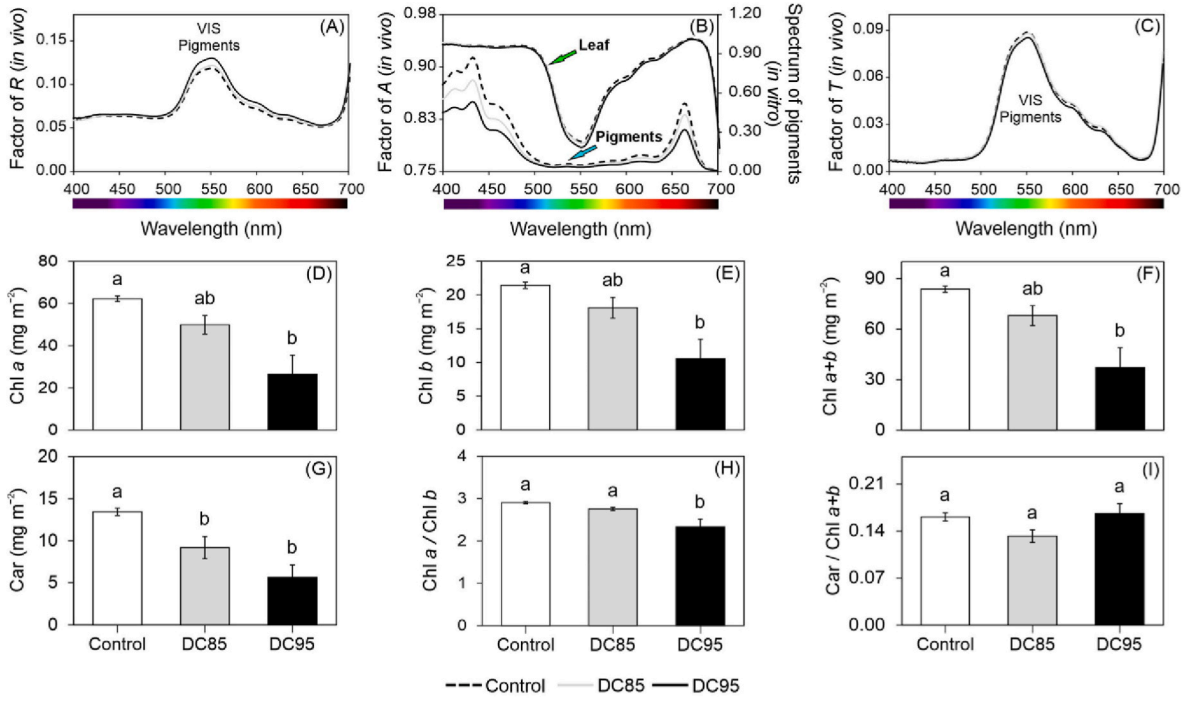

Fig. 4. Spectrum of leaves (*in vivo*) and pigments (*in vitro*) from 400 to 750 nm in cotton plants grown under distinct degree of soil compaction (DC) 75% (control), 85% (DC85), 95% (DC95). **(A)** Factor of reflectance (*R*) from 400 to 700 nm. **(B)** Factor of absorbance (*A*) and spectrum of chloroplast pigments from 400 to 700 nm. **(C)** Factor of transmittance (*T*) from 400 to 700 nm. **(D)** Chlorophyll *a* (Chl *a*) by area. **(E)** Chlorophyll *b* (Chl *b*) by area. **(F)** Total chlorophyll (Chl *a*+*b*) by area. **(G)** Carotenoids (Car) by area. **(H)** Chlorophyll *a*/*b* ratio. **(I)** carotenoids/total chlorophyll ratio (Car/Chl *a*+*b* ratio). Different letters over the bars indicate significant statistical differences between plants grown under different soil compaction conditions, as determined by Duncan's test ($p<0.05$). (n = 5 ± SE).

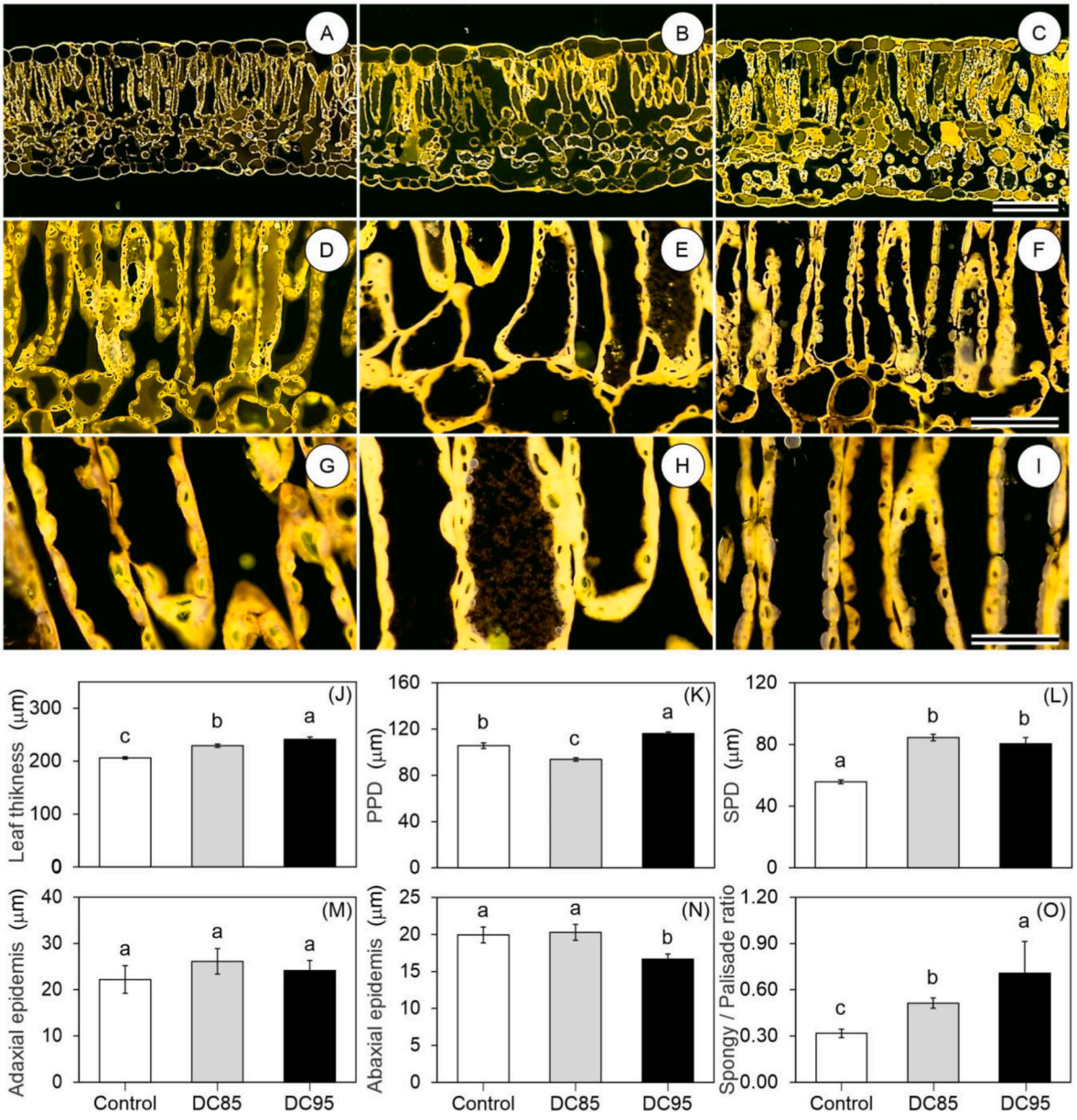

Fig. 5. Representative images of optical microscopy (OM) in top−bottom and anatomical analyses of cotton plants grown under distinct degree of compaction (DC) 75% (control), 85% (DC85), 95% (DC95). **(A-D-G)** Cross−sections of representative leaves under control. **(B-E-H)** Cross−sections of representative leaves under DC85. **(C-F-I)** Cross−sections of representative leaves under DC95. **(J)** total leaf thickness. **(K)** palisade parenchyma delimitation (PPD). **(L)** spongy parenchyma delimitation (SPD). **(M)** adaxial epidermis thickness. **(N)** abaxial epidermis thickness. **(O)** spongy/palisade parenchyma ratio. Scale bars = 150 µm and 50 µm for top and bottom, respectively. Different letters under the bars indicate significant statistical differences between plants grown under different soil compaction conditions, as determined by Duncan's test ($p<0.05$). (n = 5 ± SE).

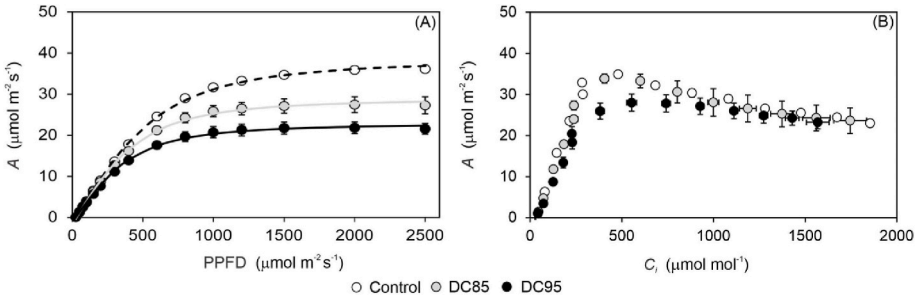

Fig. 6. Curve responses in cotton plants grown under distinct degree of compaction (DC) 75% (control), 85% (DC85), 95% (DC95). **(A)** Net photosynthesis response to light (A−PPFD). **(B)** Net photosynthesis response to CO_2 (A−C_i). (n = 5 ± SE).

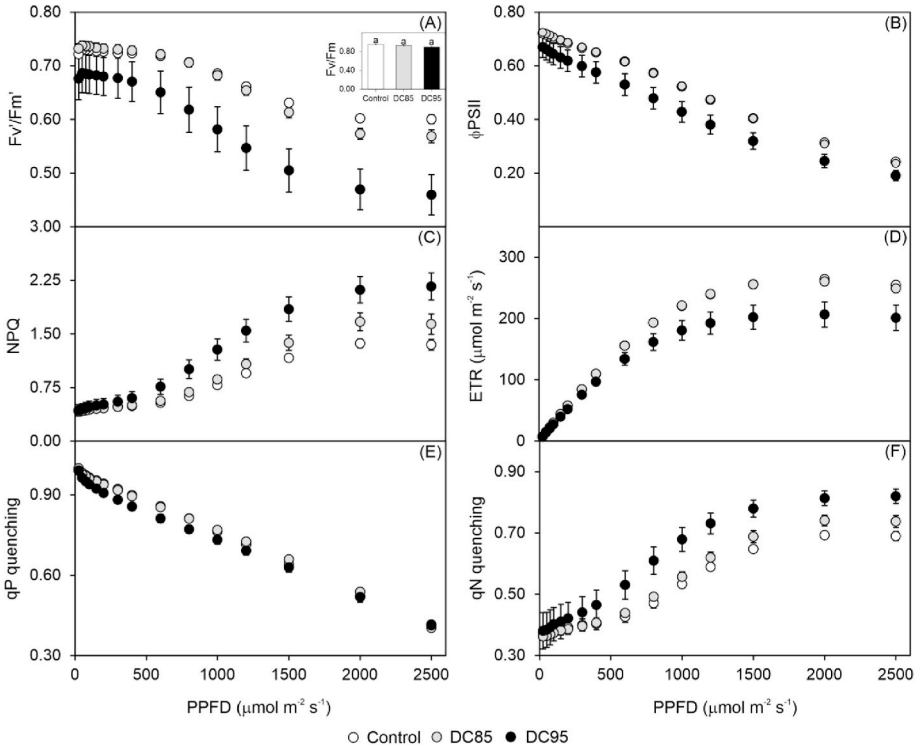

Fig. 7. Curves of fluorescence response obtained simultaneously with the photosynthetic response to light. **(A)** Effective quantum yield of PSII (Fv'/Fm'). The inset shown in the bar graph indicates the maximum quantum yield of PSII (Fv/Fm) in dark−adapted leaves. **(B)** Operational efficiency of photosystem II (ΦPSII). **(C)** Nonphotochemical quenching (NPQ). **(D)** Electron transport rate (ETR). **(E)** Photochemical dissipation quenching (qP). **(F)** Nonphotochemical dissipation quenching (qN). Different letters under the bars indicate significant statistical differences between plants grown under different soil compaction conditions, as determined by Duncan's test ($p<0.05$). (n = 5 ± SE).

Table 2
Estimated photosynthetic parameters in response to light of cotton plants grown under distinct degree of soil compaction (DC) 75% (control), 85% (DC85), 95% (DC95). Different letters at column indicate statistically significant differences between treatments by Duncan's test ($p<0.05$).

Treatment	Rd	Pg_{max}	A_{max}	LCP	LSP	α
	µmol CO_2 m^{-2} s^{-1}			µmol photons m^{-2} s^{-1}		[(µmol CO_2 m^{-2} s^{-1})/(µmol photons m^{-2} s^{-1})]
Control	1.68 ± 0.10 a	34.27 ± 0.85 a	40.02 ± 0.92 a	29.38 ± 1.75 a	1157.26 ± 31.94 a	0.06 ± 0.00 a
DC85	1.80 ± 0.19 a	25.83 ± 1.88 b	30.79 ± 2.10 b	30.92 ± 1.57 a	906.01 ± 80.88 b	0.06 ± 0.00 a
DC95	1.68 ± 0.12 a	22.30 ± 1.45 b	26.91 ± 1.71 b	31.72 ± 2.36 a	852.08 ± 37.70 b	0.05 ± 0.00 a

Dark respiration rate – Rd, maximum gross photosynthesis rate – Pg_{MAX}, maximum photosynthetic potential – A_{MAX}, light compensation point – LCP, light saturating point – LSP, and maximum quantum yield of photosynthesis – α.

constraints (Table 2). *A* and *Ci* progressively decreased in DC85 and more markedly in DC95 under both high light intensity and elevated CO_2 concentration (Fig. 6A and B), indicating stomatal and Rubisco-related limitations. VC_{MAX} was 31% lower in DC95, confirming reduced carboxylation capacity under compaction (Table 3).

Fluorescence results also revealed reduced photochemical efficiency in DC95 (Fig. 7). Fv'/Fm' and ΦPSII values were 12% and 14% lower in DC95 compared to the control (Fig. 7A and B). Concurrently, NPQ increased with compaction, especially in DC95, indicating greater energy dissipation as heat (Fig. 7C). ETR was 20% lower in DC95, with a corresponding increase in carotenoid content, highlighting their role in thermal dissipation under stress conditions (Fig. 7D–F).

3.8. Chlorophyll *a* fluorescence transient evaluation

Difference kinetics of the OJIP transients (ΔVt, expressed relative to the Control) were used to highlight the characteristic features of the fast fluorescence rise, including the L-band (~150 µs), K-band (~300 µs), and the J (~2 ms), I (~30 ms) and P (~300 ms) steps (Fig. 8A and B).

In DC95, a positive L-band indicates reduced energetic connectivity (ungrouping) among PSII units, consistent with disturbed excitation energy sharing within PSII. The positive K-band in DC95 suggests donor-

Table 3
Estimated photosynthetic parameters in response to CO_2 of cotton plants grown in soil under distinct degree of compaction (DC) 75% (control), 85% (DC85), 95% (DC95). Different letters at column indicate statistically significant differences between treatments by Duncan's test ($p<0.05$).

		Control	DC85	DC95
VC_{MAX}	µmol CO_2 m^{-2} s^{-1}	124.87 ± 2.44 a	114.91 ± 15.44 ab	86.33 ± 12.53 b
J_{MAX}	µmol photons m^{-2} s^{-1}	143.17 ± 3.91 a	141.98 ± 11.19 a	128.2 ± 9.78 a
TPU	µmol CO_2 m^{-2} s^{-1}	8.10 ± 0.25 a	8.13 ± 1.03 a	8.03 ± 0.56 a

Maximum carboxylation rate of Rubisco VC_{MAX}, maximum rate of electron transport for the given light intensity – J_{MAX}, triose phosphate use limitation – TPU.

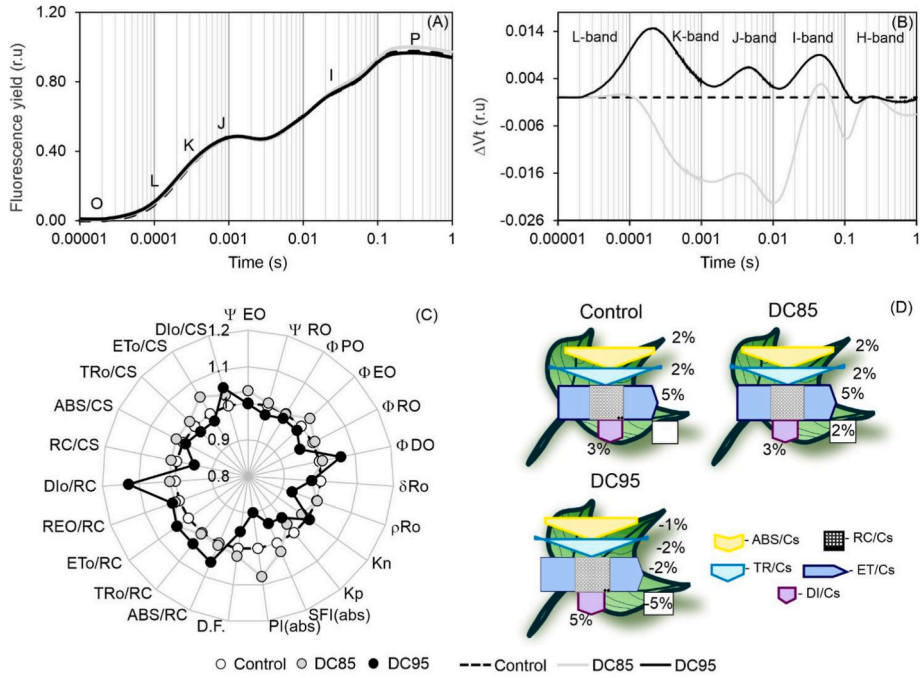

Fig. 8. Chlorophyll *a* fluorescence kinetics parameters derivative of JIP−test in cotton plants grown under distinct degree of compaction (DC) 75% (control), 85% (DC85), 95% (DC95). **(A)** Chlorophyll *a* fluorescence induction kinetics with normalized data. **(B)** Variable fluorescence kinetics of standardised chlorophyll (ΔVt = (Ft − F0)/Fv) − Vt control). The L-band, K-band, J-band, I-band, and H-band relative changes in variable fluorescence over time reflect alterations in the efficiency of the light−harvesting complexes (LHCs), active reaction centres (RCs), and energy flow in the electron transport chain between PSII and PSI. **(C)** Radar plot indicating parameters derived from the chlorophyll *a* fluorescence kinetics transient (JIP−test). **(D)** pipeline leaf displays phenomenological energy flow through excited cross sections (CSs) of leaves. Yellow arrow−ABS/CS, absorption flow by approximate CS; light blue arrow−TR/CS, energy flow trapped by CS; blue arrow−ET/CS, electron transport flow by CS; purple arrow−DI/CS, energy flow dissipated by CS; circles inscribed in squares−RC/CS, indicate the % of active/inactive reaction centres. The white circles inscribed in squares represent reduced (active) Q_A reaction centres, black circles represent nonreducing (inactive) Q_A reaction centres, and 100% of the active reaction centres responded with the highest average numbers observed in relation to the control. Arrow sizes indicate the changes in energy flows compared to control. Different asterisks or letters inside the arrow indicate significant differences between plants grown under different compaction conditions, as determined by Duncan's test ($p<0.05$). The standard error was omitted for clarity.

side impairment of PSII, consistent with decreased stability/activity of the oxygen-evolving complex. DC95 also showed an enhanced signal at the J-step, indicating a higher accumulation of Q_A^- and therefore a restriction of electron transfer beyond Q_A (towards Q_B and the plastoquinone pool).

At the I-step (~30 ms), both compacted treatments deviated from the Control, indicating altered reduction kinetics of the plastoquinone pool and/or intersystem electron carriers. In the I–P phase, no clear treatment effect was detected around the H feature (~100 ms), suggesting that the late phase of the transient was not markedly differentiated among treatments under our conditions (Fig. 8A and B).

3.9. JIP−Test parameters and thermal analysis

Soil compaction impaired the electron transport efficiency in PSII, particularly in the DC95 treatment (Fig. 8C–E). In DC95, ψ_{EO} (probability that an electron in PSII is transferred from Q_A^- to the plastoquinone pool at the PSII acceptor side) and ψ_{RO}, (probability that an electron reaches the final electron acceptors at the PSI acceptor side) were both reduced, indication restriction in electron flow from PSII towards PSI. Similarly, φ_{EO} and φ_{RO}, the quantum yields for electron transport beyond Q_A^- and for the reduction of PSI end acceptors, respectively, also decreased under DC95. Moreover, δ_{RO} and ρ_{RO}, which describe the efficiency with which electrons are transferred from the intersystem carriers to the final acceptors on the PSI acceptor side, showed decreasing trends in DC95. Notably, the increase in DC95 suggests enhanced energy dissipation under compaction (Fig. 8C).

Fluorescence indices such as SFI(abs) and PI(abs) were reduced in DC95 but increased in DC85, indicating lower PSII performance and higher thermal dissipation in DC95 (Fig. 8C). This is supported by elevated ABS/RC and DIo/RC values, pointing to greater energy absorption and dissipation demands. Additionally, the RC/CS, ABS/CS, TRo/CS, ETo/CS, and DIo/CS parameters confirm that compaction reduces PSII efficiency and increases the need for protective energy dissipation mechanisms in DC95 leaves (Fig. 8D).

3.10. Alterations in chloroplast ultrastructures

Plants grown in compacted soil (DC85 and DC95) showed an average of 16 chloroplasts per cell in the palisade parenchyma, 24% fewer compared to the control (21 chloroplasts) (Fig. 9A–R). In contrast, the spongy parenchyma exhibited a 20% increase in chloroplast number in the compacted treatments (DC85 and DC95) relative to the control (Fig. 9A–R). Chloroplast distribution within cell structures also varied with soil compaction (Fig. 9A–O). The ratio of chloroplasts in the spongy to palisade parenchyma increased by 39% in DC85 and 56% in DC95 compared to the control (Fig. 9R). From a morphological perspective, thylakoids in the DC85 treatment were thinner and more elongated, with less stacking compared to the control. In the DC95 treatment, accentuated features were observed with thylakoids more elongated, thinner, and had less stacking, but with greater formation of stromal thylakoids (Fig. 9O).

3.11. Carbohydrate alterations

Glucose, fructose, and sucrose contents were significantly reduced with increasing soil compaction (DC85 and DC95; Fig. 10), as well as the amount of starch in the chloroplasts (Fig. 9A–O and 10D).

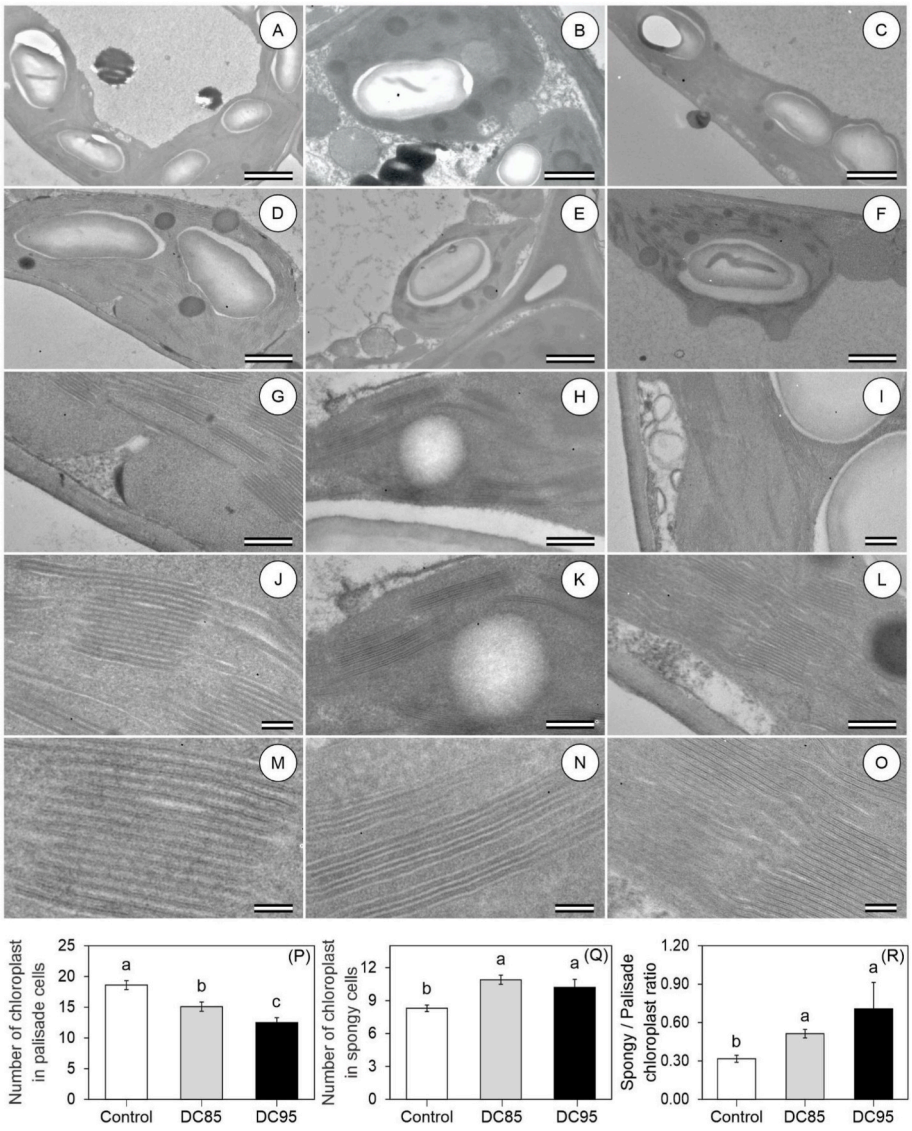

Fig. 9. Representative image of transmission electron microscopy (TEM) of chloroplasts in the palisade parenchyma of cotton plants grown under distinct degree of compaction (DC) 75% (control), 85% (DC85), 95% (DC95). **(A, D, G, J, M)** Control. **(B, E, H, K, N)** DC85. **(C, F, I, L, O)** DC95. **(P)** Number of chloroplasts in palisade cells. **(Q)** Number of chloroplasts in spongy cells. **(R)** Spongy/palisade chloroplast ratio. Scale bar = 1 μm for (A–D) and 200 nm for (E–T), respectively. Different letters under the bars indicate significant differences between plants grown under different compaction conditions, as determined by Duncan's test ($p<0.05$). (n = 5 ± SE).

3.12. Principal component analysis

Principal component analysis (PCA) investigates the relationship between different levels of soil compaction and total dry matter accumulation in cotton plants (Fig. S5). The first two principal components accounted for 52.3% of the total variance, with PC1 and PC2 explaining 45.9% and 13.7%, respectively. Collectively, PCA data suggest that soil compaction influences total dry matter accumulation in cotton plants in a complex manner, and PC1 and PC2 explain multidimensional patterns, aligning various parameters associated with soil physical properties (16% and 8%), primary growth (19.9% and 2.1%) and derivatives (10.8% and 10.5%), leaf pigments (14.9% and 10.1%), leaf optical properties (3.4% and 5.8%), photochemical (9% and 13.6%), carboxylation (7.2% and 7.6%), fluorescence (10.3% and 5.1%), nutritional (1.7% and 16.6%), and structural and ultrastructural changes (6.7% and 20.6%), ultimately reflecting dry matter accumulation in plants.

4. Discussion

4.1. Growth response to soil compaction levels

Although soil compaction is a well-known factor affecting plant growth (Kozlowski, 1999; Cambi et al., 2017), only a few studies have assessed its impact from agronomic, physiological, and structural perspectives (Cambi et al., 2017). Considering several physiological processes, this study investigated the response of cotton plant growth to soil compaction in a sandy-textured soil under three compaction levels – non-compacted (DC75), intermediate compacted (DC85), and highly compacted (DC95), without water and nutrient limitations. Increasing soil compaction decreased soil physical quality and limited below- and above-ground plant growth (Fig. 1), decreasing root expansion and its capacity to occupy soil pores. While soil compaction increased, carbon accumulation shifted from root biomass towards above-ground biomass (Figs. 1–2), but leaf growth and its capacity to promote C gain decreased due to the reduced ULR values (Fig. 2H), which is aligned with previous

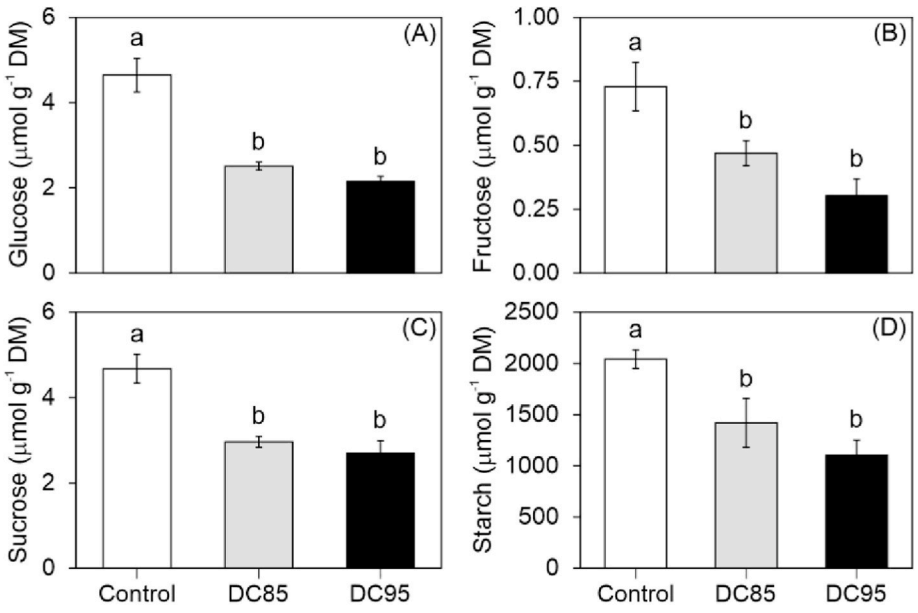

Fig. 10. Glucose (A), fructose (B), sucrose (C) and starch (D) contents in cotton leaves from plants grown in soil under distinct degree of compaction (DC) 75% (control), 85% (DC85), 95% (DC95). Different letters under the bars indicate significant statistical differences between plants grown under different compaction soil conditions, as determined by Duncan's test ($p < 0.05$). (n = 5 ± SE).

assessments (Cambi et al., 2017; Colombi and Keller, 2019; Correia et al., 2019; Huntenburg et al., 2021). The shift in carbon from roots to leaves was used for the build-up of thicker leaf tissue (Fig. 5A–C). The formation of thicker leaves under soil compaction represents an acclimatory response of plants to the mechanical and water stress imposed by this physical constraint. Compacted soils reduce porosity and hinder root system expansion, thereby limiting overall plant growth. In this context, increased leaf thickness is associated with enhanced water storage capacity in the tissues, particularly in the parenchyma, as a strategy to maintain physiological functions during periods of water limitation. However, this adaptation entails higher construction costs per unit leaf area, requiring greater structural biomass investment to develop thicker and more resistant tissues. Consequently, the efficiency of converting invested biomass into effective plant biomass gain is reduced, revealing a trade-off between growth and stress tolerance (Niinemets, 2023).

It has been argued that the overall negative impact of soil on plant performance relies on the higher soil resistance to root penetration under compaction (Colombi and Keller, 2019; Rivera et al., 2019). However, the mechanism of how soil compaction affects plant development is complex. Previous controlled studies with wheat (*Triticum aestivum*) and field trials involving sunflower (*Helianthus annuus*) demonstrated that compacted soils can markedly inhibit leaf expansion and early seedling development, even under non-limiting conditions of water, oxygen, and nutrients (Wolfe et al., 1995), which we also proved to be true for cotton plants. Throughout the diurnal measurements, reduced g_s (Fig. 3) and pronounced diffusional limitations to CO_2 entry were associated with soil compaction. Under higher compaction levels (DC85 and DC95), plants exhibited lower net photosynthetic rates and experienced reduced transpiration (Fig. 2B).

4.2. Leaf optical, morphological, and structural properties modify daily gas exchange

Soil compaction lowers light absorption by the leaves. The average leaf absorption indices (400–700 nm) ranged from 0.90 (control) to 0.85 (DC95). In addition, reduced pigment concentrations were found under compaction, which affects light reactions (Fig. 4 and S3). The leaf morphological modifications under compaction were also associated with modifications palisade to spongy ratio, stomatal density, and stomatal size (Fig. 5O and S4). Enhanced leaf thickness plays an important role in optimizing light absorption, especially in the green spectrum (Falcioni et al., 2017, 2023a; Zhen and Bugbee, 2020). However, structural traits such as an expanded spongy mesophyll primarily facilitated deeper penetration of green light, while the absorption of blue and red wavelengths remained limited to the upper leaf layers. (Zhang and Folta, 2012; Zhen and Bugbee, 2020; Liu and Van Iersel, 2021; Falcioni et al., 2023a). Despite the reduced chlorophyll concentrations (Fig. 4 and S3), the leaf optical profile indicates that there were no changes in the absorption of blue and red light. It is important to note that the modifications occurring with soil compaction were not influenced by nutrient absorption (Table S1).

Hyperspectral data revealed that increasing soil compaction decreased leaf light absorbance (Fig. 4 and S3), primarily due to enhanced reflectance rather than increased transmittance. This pattern indicates that less light was absorbed by photosynthetic pigments, thereby limiting photosynthetic efficiency, as also noted by Falcioni et al. (2023a). The reduction in pigment quantities in the most compacted soil was associated with a 16% increase in reflectance compared to the control treatment (Fig. 4 and S3). However, no reduction in chlorophyll to carotenoid ratio (Fig. 4I) was observed, providing evidence that excessive reactive oxygen species were not produced. A few pigments confined content within the thylakoid's membranes on deformed chloroplast ultrastructure (Fig. 9), as discussed later (topic 4.4). As a result, the optical leaf characteristics are altered.

4.3. Reduction of photochemical and carboxylative parameters and increases in thermal and fluorescence parameters

The detrimental effects of soil compaction on plant morphology are closely linked to disruptions in key physiological processes in cotton. Compacted soils interfere with plant metabolism by limiting photosynthetic activity, reducing leaf expansion, and slowing overall growth (Cambi et al., 2017; Colombi and Keller, 2019; Correia et al., 2019; Huntenburg et al., 2021). Although some studies have found no significant decline in photosynthesis following compaction (Andrade et al., 1993), our findings indicate a clear reduction in photosynthetic efficiency under compacted conditions (Fig. 6). This discrepancy likely

reflects technological advances in modern gas-exchange and chlorophyll fluorescence instrumentation, which provide higher sensitivity and allow the detection of subtle physiological impairments that older methodologies could not resolve. This decline in *A* appears to be driven by both stomatal and non-stomatal limitations. Notably, increased stomatal closure under severe compaction likely restricted CO_2 diffusion into the mesophyll (Cambi et al., 2017; Mariotti et al., 2020), as supported by the observed rise in stomatal limitation. Furthermore, photosynthetic capacity may have also been constrained at the chloroplast level, potentially due to decreased biochemical efficiency (*e.g.*, VC_{MAX}).

A decrease of 32.76% in A_{MAX} and 26% in LSP, observed in the most compacted soil, DC95 (Fig. 6A and B, Table 2), indicates that the photosynthetic apparatus was damaged. The damage of cellular metabolism (e.g., reduction in LSP) suggests an inability to use light efficiently, damaging the light-harvesting system and the electron transport chain (Falcioni et al., 2023b). Rubisco activity is compromised by soil compaction, with a tendency for compromised triose-phosphate synthesis due to damage not only to photochemical reactions (Table 2) but also to the reduction of VC_{MAX} in carboxylative reactions (Table 3).

Our results indicate a 21% reduction in carbon assimilation at light saturation in the DC95 treatment compared to the control (Fig. 6B), reflecting increased energy demands for tissue formation and the maintenance of cellular and photosynthetic functions. The upregulation of energy dissipation mechanisms, particularly the xanthophyll cycle, suggests that soil compaction enhances non-photochemical quenching (NPQ) (Fig. 7C), while simultaneously decreasing the efficiency of energy utilization via photochemical quenching (ΦPSII, qP) (Fig. 7B–E). NPQ, which mediates thermal dissipation of excess excitation energy within the antenna complex (Fig. 7C), becomes more pronounced under reduced electron transport rates (ETR) (Fig. 7D). This response is often accompanied by a decline in carotenoid levels, limiting the plant's capacity to dissipate excess energy and indicating a state of oxidative or thermal stress. Under these conditions, impaired energy dissipation can lead to a feedback loop that exacerbates damage to the antenna complex and triggers photoinhibition (Falcioni et al., 2023b).

Both *A and* reduced g_s impact *E* (Fig. S1). Higher *i*WUE – the amount of carbon assimilated per unit of water transpired (*A*/E; Lawson and Blatt, 2014) – under compacted soil (DC95; Fig. S2) reflects the inverse relationship between *i*WUE and g_s. However, gains in *i*WUE under compaction are usually associated with lower *A* and reduced plant growth. Plants exhibiting higher g_s typically have greater carbon assimilation and faster growth under favorable conditions but exhibit lower water use efficiency because cotton, a C_3 plant, must maintain stomata opening to acquire CO_2 for photosynthesis, thereby resulting in water loss. Moreover, reduced g_s decreases transpiration at the expense of carbon gain in C_3 species (Lawson and Blatt, 2014). The observed reduction in transpiration under compacted soil may also inhibit evaporative cooling, leading to increased leaf temperature and potential exacerbation of photoinhibition. Previous studies suggest that the decline in leaf photosynthesis under soil compaction is often linked to limited water and nutrient uptake due to restricted root growth (Mariotti et al., 2020). In our study, however, plants were grown under non-limiting water and nutrient conditions, and reductions in g_s, along with *A* and *E*, were observed consistently throughout the day (Fig. 3 and S1). Possibly, under compacted conditions, plants can regulate the stomatal aperture to allow only enough CO_2 influx to match the limited carboxylation capacity, thereby avoiding excessive *Ci* accumulation. This behavior represents a homeostatic response that maintains internal CO_2 balance under metabolic constraints, reflecting a coordinated regulation between stomatal conductance and the biochemical capacity for photosynthesis.

The quantum yields of primary photochemistry (Φ_{PO}) and electron transfer from Q_A to PQ (Φ_{EO}) were slightly affected by soil compaction. Similarly, the quantum yield for heat dissipation (Φ_{DO}) increased with soil compaction. We can speculate that reduction in electrons transfer speed from Q_A to Q_B or PQ pool associated to lower values of ψ_{EO} and ψ_{RO} Q_A to PQ should be associated to accumulation of 2-phosphoglycolate (2-PG, a product of oxygenation of RUBP from Rubisco, or photorespiration process) since 2-PG is considered an inhibitor of electron transfer from Q_A to Q_B (Zelitch et al., 2009). PI(abs) is a valuable indicator for evaluating photosynthetic performance and identifying the effects of abiotic stress on PSII across various plant species (Ghaffar et al., 2023). This index integrates information on the number of active chlorophyll reaction centres, the efficiency of energy capture, and electron transport from PSII to the plastoquinone pool, processes that are closely associated with NADPH production (Botyanszka et al., 2020). Under severe soil compaction (DC95), increases in energy absorption (ABS/RC), energy trapping (TRo/RC), and electron transport flux (ETo/RC) per reaction center were observed (Fig. 8). These patterns suggest that cotton plants subjected to DC95 were unable to regulate antenna size properly, resulting in damage to active PSII centres likely due to excessive photochemical stress (Strasser et al., 2000). As a result, a larger portion of the absorbed energy was dissipated as heat (DIo/RC), probably as a compensatory response to the impaired electron transport chain (ETR) (Fig. 8).

4.4. Comparative analysis of chloroplast to energy yield

The comparative analysis of chloroplast ultrastructure under compaction presents significant implications for photosynthesis associated with energy production in plants. We observed that soil compaction conditions induce different adaptive mechanisms in chloroplasts (Fig. 9), associated with energy conversion based on NADH, NADPH, and ATP.

Chloroplast ultrastructure analyses indicate that compaction induced marked changes in the organization of the photosynthetic apparatus, which can help explain the functional constraints detected by gas exchange and fluorescence. In compacted soils (DC85 and DC95), the reduced number of chloroplasts in palisade mesophyll cells and the altered thylakoid stacking are consistent with lower light harvesting capacity and reduced efficiency of electron transport, ultimately contributing to decreased carbohydrate accumulation. Notably, because the H-band did not differ among treatments in our dataset (Fig. 8), the primary fluorescence signatures of compaction are more consistently interpreted from earlier (L/K) and mid-phase (J/I) alterations, in combination with the independent anatomical and ultrastructural evidence.

Under compacted soils, DC85 and DC95, the reduced number of chloroplasts in the palisade mesophyll results in moderate energy yield per leaf and plant (Fig. 9). The lower energy production can modulate the distribution between photosynthesis and daily respiration, allowing maintenance of metabolic processes (Pinelli and Loreto, 2003; Casella et al., 2017; Coelho et al., 2017). This can be evidenced in DC95, aligned with an increase in stroma lamellae, adjusting the balance for ATP formation and NADPH production in photosystem I (PSI) (Shikanai, 2014; Shikanai and Yamamoto, 2017). This stromal arrangement of thylakoids may be an adaptive mechanism to maintain energy directed to the Calvin-Benson cycle. For example, the slight reduction in H-band compared to the control highlights these structural changes (Fig. 8).

The triggering leaves don't have a significant impact on the rate and extent of variable fluorescence in the photochemical O-J phase for CO_2 reduction in the chloroplast stroma or the use of carbon skeletons in daily respiration (Pinelli and Loreto, 2003; Toshoji et al., 2012). This highlights the resilience of the reactions responsible for variable fluorescence in the face of potential damage to the permeability of cellular membranes. Interestingly, the I-P phase shows lower electron transport rates (Fig. 8), indicating that cellular activities, such as the propagation of action potentials along thylakoid membranes, could reduce photosynthetic activity (Miao et al., 2016; Gao et al., 2018; Samborska et al., 2019). Under DC85 and DC95 conditions, we observed a significant reduction in the number of chloroplasts, indicating a reduction in photosynthetic activity. Chloroplasts under these conditions show an

increase in stromal lamellae, pointing to higher reducing power in PSI, with signs of a reduction or loss of final formed reducing power, contributing to a decrease in overall energy yield (Fig. 9, Table 2).

The overall changes in chloroplast functioning altered end-products of photosynthesis such as glucose, fructose, sucrose, and starch (Fig. 10). The sugar metabolic pathway was compromised, consistent with the observed carboxylative rates and Rubisco efficiency in CO_2 fixation for DC85 and DC95. Our results showed that soil compaction affects cotton growth due to changes in photosynthetic machinery, with photochemical and carboxylative damage. Despite lower plant growth under compaction (Fig. 1), there is no evidence of direct end-product-mediated feedback down-regulation of photosynthesis or sugar accumulation associated with source-sink relationship (DaMatta et al., 2008; Ronchi et al., 2006). Instead, reduced sugar content was associated with a limited photosynthetic rate, and there was no direct evidence of limited translocation phloem (Burkle et al., 1998).

5. Conclusions

This study demonstrates that soil compaction impairs cotton growth and photosynthetic performance even under non-limiting water and nutrient conditions. By degrading key soil physical properties and processes, soil compaction constrains root growth and modifies biomass allocation. The reduction in stomatal conductance, net carbon assimilation, and transpiration, alongside unaltered *Ci* values and reduced Rubisco activity, highlights a combined limitation of both diffusional and biochemical processes involved in photosynthesis. Furthermore, changes in leaf optical properties, reductions in pigment concentrations, chloroplast number, and thylakoid structure, as well as increased thermal dissipation and altered fluorescence kinetics, indicate that soil compaction affects the photosynthetic machinery at multiple levels. These alterations result in decreased carbon fixation capacity and lower carbohydrate accumulation. Finally, our findings emphasize that soil compaction is not merely a physical constraint but a multidimensional stress that integrates mechanical, and biochemical limitations, ultimately reducing plant productivity. This highlights the need for soil management strategies that preserve or restore soil structure to sustain cotton yield potential in mechanized agriculture systems.

CRediT authorship contribution statement

Camila P. Cagna: Writing – original draft, Visualization, Project administration, Methodology, Investigation, Formal analysis, Data curation, Conceptualization. **Cássio A. Tormena:** Writing – review & editing, Supervision, Resources, Project administration, Funding acquisition. **Renan Falcioni:** Writing – original draft, Visualization, Methodology, Investigation, Formal analysis, Data curation, Conceptualization. **Fabio R. Echer:** Writing – review & editing, Resources. **Olanrewaju H. Ologunde:** Writing – original draft. **Marcio R. Nunes:** Writing – review & editing, Supervision, Resources. **Werner C. Antunes:** Writing – review & editing, Writing – original draft, Supervision, Resources.

Declaration of competing interest

The authors declare that they have no known competing financial interests or personal relationships that could have appeared to influence the work reported in this paper.

Acknowledgements

The authors are grateful to CNPq (Conselho Nacional de Desenvolvimento Científico e Tecnológico) for providing scholarships. This study was financed in part by the Coordenação de Aperfeiçoamento de Pessoal de Nível Superior – Brazil (CAPES) - Finance Code 001. We also thank the USDA National Institute of Food and Agriculture, Research Capacity Fund (Hatch) project 7004188 (Hatch grant FLA-SWS-006289 to MRN).

Appendix A. Supplementary data

Supplementary data to this article can be found online at https://doi.org/10.1016/j.plaphy.2026.111064.

Abbreviations

A –	net photosynthesis
A_{MAX} –	maximum photosynthetic potential
AC –	air capacity
AC/TP –	air storage capacity
α –	maximum quantum yield of photosynthesis
Ca –	calcium
Car –	carotenoids
Chl *a* –	chlorophyll *a*
Chl *a*+*b* –	total chlorophyll
Chl *b* –	chlorophyll *b*
Ci –	internal CO_2 concentration
Cu –	copper
DC –	degree of compaction
E –	net transpiration rate
ETR –	electron transport rate
FC –	field capacity
FC/TP –	water storage capacity
Fe –	iron
Fv/Fm –	maximum quantum yield of PSII
Fv'/Fm' –	effective quantum yield of PSII
g_s –	stomatal conductance
*i*WUE –	intrinsic water use efficiency
J_{MAX} –	maximum rate of electron transport for the given light intensity
K –	potassium
K_{air} –	air permeability
LAR –	leaf area ratio
LCP –	light compensation point
LMF –	leaf mass fraction
LSP –	light saturating point
Macro –	macroporosity
Meso –	mesoporosity
Mg –	magnesium
Micro –	microporosity
Mn –	manganese
N –	nitrogen
NPQ –	nonphotochemical quenching
P –	phosphorus
PAW –	plant available water
Pg_{MAX} –	maximum gross photosynthesis rate
PPD –	palisade parenchyma delimitation
PWP –	permanent wilting point
qN –	nonphotochemical dissipation quenching
qP –	photochemical dissipation quenching
Rd –	dark respiration rate
RMF –	root mass fraction
RPFC –	penetration resistance in field capacity
SLA –	specific leaf area
SMF –	stem mass fraction
SPD –	spongy parenchyma delimitation
TP –	total porosity
TPU –	triose phosphate use limitation
URL –	unit leaf rate
VC_{MAX} –	maximum carboxylation rate of Rubisco
WPT –	whole plant transpiration
WUE –	water use efficiency
Zn –	zinc

$\theta_{2\ MPa}$ – critical moisture content
ΦPSII – operational efficiency of photosystem II

Data availability

Data will be made available on request.

References

Andrade, A., Wolfe, D.W., Fereres, E., 1993. Leaf expansion, photosynthesis, and water relations of sunflower plants grown on compacted soil. Plant Soil 149, 175–184. https://doi.org/10.1007/BF00016607.

Anghinoni, G., Tormena, C.A., Lal, R., Zancanaro, L., Kappes, C., 2019. Enhancing soil physical quality and cotton yields through diversification of agricultural practices in central Brazil. Land Degrad. Dev. 30, 788–798. https://doi.org/10.1002/ldr.3267.

Baker, N.R., Harbinson, J., Kramer, D.M., 2007. Determining the limitations and regulation of photosynthetic energy transduction in leaves. Plant Cell Environ. 30, 1107–1125. https://doi.org/10.1111/j.1365-3040.2007.01680.x.

Ball, B.C., Schjonning, P., 2002. Air permeability. In: Methods of Soil Analysis. Soil Science Society of America, Madison, Wisconsin, pp. 1141–1158. https://doi.org/10.2136/sssabookser5.4.c46.

Blainski, É., Tormena, C.A., Fidalski, J., Guimarães, R.M.L., 2008. Quantificação da degradação física do solo por meio da curva de resistência do solo à penetração. Rev. Bras. Ciência do Solo 32, 975–983. https://doi.org/10.1590/S0100-06832008000300007.

Blake, G.R., Hartge, K.H., 1986. Bulk density. In: Klute, A. (Ed.), Methods of Soil Analysis: Part. 1 Physical and Mineralogical Methods, 1.1. Am Soc of Agron, pp. 363–382. https://doi.org/10.2136/sssabookser5.1.2ed.c13.

Burkle, L., Hibberd, J.M., Quick, W.P., Kühn, C., Hirner, B., Frommer, W.B., 1998. The H +-sucrose cotransporter NtSUT1 is essential for sugar export from tobacco leaves. Plant Physiol. 118 (1), 59–68. https://doi.org/10.1104/pp.118.1.59.

Botyanszka, L., Zivcak, M., Chovancek, E., Sytar, O., Barek, V., Hauptvogel, P., 2020. Chlorophyll fluorescence kinetics may be useful to identify early drought and irrigation effects on photosynthetic apparatus in field-grown wheat. Agronomy 10, 1275. https://doi.org/10.3390/agronomy10091275.

Cambi, M., Hoshika, Y., Mariotti, B., Paoletti, E., Picchio, R., Venanzi, R., Marchi, E., 2017. Compaction by a forest machine affects soil quality and Quercus robur L. seedling performance in an experimental field. For. Ecol. Manag. 384, 406–414. https://doi.org/10.1016/j.foreco.2016.10.045.

Casella, S., Huang, F., Mason, D., Zhao, G.Y., Johnson, G.N., Mullineaux, C.W., Liu, L.N., 2017. Dissecting the native architecture and dynamics of cyanobacterial photosynthetic machinery. Mol. Plant 10, 1434–1448. https://doi.org/10.1016/j.molp.2017.09.019.

CCA, 2020. Qualitative Report on the 2019-20 Cotton Season: a Survey of Consultants. Crop Consultants, Australia.

Coelho, É.M.P., Barbosa, M.C., Mito, M.S., Mantovanelli, G.C., Oliveira, R.S., Ishii-Iwamoto, E.L., 2017. The activity of the antioxidant defense system of the weed species Senna obtusifolia L. and its resistance to allelochemical stress. J. Chem. Ecol. 43, 725–738. https://doi.org/10.1007/s10886-017-0865-5.

Colombi, T., Keller, T., 2019. Developing strategies to recover crop productivity after soil compaction—A plant eco-physiological perspective. Soil Tillage Res. 191, 156–161. https://doi.org/10.1016/j.still.2019.04.008.

Correia, J., Postma, J.A., Watt, M., Wojciechowski, T., 2019. Soil compaction and the architectural plasticity of root systems. J. Exp. Bot. 70, 6019–6034. https://doi.org/10.1093/jxb/erz383.

Daloso, D.M., Antunes, W.C., Pinheiro, D.P., Waquim, J.P., Araújo, W.L., Loureiro, M.E., Williams, T.C., 2015. Tobacco guard cells fix CO2 by both Rubisco and PEP case while sucrose acts as a substrate during light-induced stomatal opening. Plant Cell Environ. 38, 2353–2371. https://doi.org/10.1111/pce.12555.

DaMatta, F.M., Cunha, R.L., Antunes, W.C., Martins, S.C., Araujo, W.L., Fernie, A.R., Moraes, G.A., 2008. In field-grown coffee trees source–sink manipulation alters photosynthetic rates, independently of carbon metabolism, via alterations in stomatal function. New Phytol. 178 (2), 348–357. https://doi.org/10.1111/j.1469-8137.2008.02367.x.

De Jong Van Lier, Q., Logsdon, S.D., Pinheiro, E.A.R., Gubiani, P.I., 2023. Plant available water. In: Goss, M.J., Oliver, M. (Eds.), Encycl of Soils in the Environ. Acad Press, pp. 509–515.

Falcioni, R., Antunes, W.C., Demattê, J.A.M., Nanni, M.R., 2023a. A novel method for estimating chlorophyll and carotenoid concentrations in leaves: a two hyperspectral sensor approach. Sensors 23, 3843. https://doi.org/10.3390/s23083843, 2023.

Falcioni, R., Moriwaki, T., Bonato, C.M., de Souza, L.A., Nanni, M.R., Antunes, W.C., 2017. Distinct growth light and gibberellin regimes alter leaf anatomy and reveal their influence on leaf optical properties. Environ. Exp. Bot. 140, 86–95. https://doi.org/10.1016/j.envexpbot.2017.06.001.

Falcioni, R., Moriwaki, T., Benedito, E., Bonato, C.M., de Souza, L.A., Antunes, W.C., 2018. Increased gibberellin levels enhance light capture efficiency in tobacco plants and promote dry matter accumulation. Theor. Experiment Plant Physiol. 30, 235–250. https://doi.org/10.1007/s40626-018-0118-1.

Falcioni, R., Moriwaki, T., Rodrigues, M., de Oliveira, K.M., Furlanetto, R.H., dos Reis, A. S., Antunes, W.C., 2023b. Nutrient deficiency lowers photochemical and carboxylation efficiency in tobacco. Theor. Experiment Plant Physiol. 35, 91–97. https://doi.org/10.1007/s40626-023-00268-2.

Flint, A.L., Flint, L.E., 2002. Particle density. In: Methods of Soil Analysis: Part 4 Physical Methods. Soil Science Society of America, Madison, Wisconsin, pp. 229–240. https://doi.org/10.2136/sssabookser5.4.c10.

Gao, Y., Liu, W., Wang, X., Yang, L., Han, S., Chen, S., Qiang, S., 2018. Comparative phytotoxicity of usnic acid, salicylic acid, cinnamic acid and benzoic acid on photosynthetic apparatus of Chlamydomonas reinhardtii. Plant Physiol. Biochem. 128, 1–12. https://doi.org/10.1016/j.plaphy.2018.04.037.

Ghaffar, A., Hussain, N., Ajaj, R., Shahin, S.M., Bano, H., Javed, M., Athar, H.U.R., 2023. Photosynthetic activity and metabolic profiling of bread wheat cultivars contrasting in drought tolerance. Front. Plant Sci. 14, 1123080. https://doi.org/10.3389/fpls.2023.1123080.

Grable, A.R., Siemer, E.G., 1968. Effects of bulk density, aggregate size, and soil water suction on oxygen diffusion, redox potentials, and elongation of corn roots. Soil Sci. Soc. Am. J. 32 (2), 180–186. https://doi.org/10.2136/sssaj1968.03615995003200020011x.

Hamza, M.A., Anderson, W.K., 2005. Soil compaction in cropping systems: a review of the nature, causes and possible solutions. Soil Tillage Res. 82 (2), 121–145. https://doi.org/10.1016/j.still.2004.08.009.

Hoffmann, W.A., Poorter, H., 2002. Avoiding bias in calculations of relative growth rate. Ann. Bot. 90, 37–42. https://doi.org/10.1093/aob/mcf140.

Huntenburg, K., Dodd, I.C., Stalham, M., 2021. Agronomic and physiological responses of potato subjected to soil compaction and/or drying. Ann. Appl. Biol. 178 (2), 328–340. https://doi.org/10.1111/aab.12675.

Jamali, H., Nachimuthu, G., Palmer, B., Hodgson, D., Hundt, A., Nunn, C., Braunack, M., 2021. Soil compaction in a new light: know the cost of doing nothing–A cotton case study. Soil Tillage Res. 213, 105158. https://doi.org/10.1016/j.still.2021.105158.

Jolliffe, I.T., 2002. Principal Component Analysis for Special Types of Data. Springer, New York, pp. 338–372.

Karnovsky, M.J., 1965. A formaldehyde-glutaraldehyde fixative of high osmolality for use in electron-microscopy. JCB (J. Cell Biol.) 27, 137–138A. https://doi.org/10.4236/ajps.2019.105051.

Keller, T., Sandin, M., Colombi, T., Horn, R., Or, D., 2019. Historical increase in agricultural machinery weights enhanced soil stress levels and adversely affected soil functioning. Soil Tillage Res. 194, 104293. https://doi.org/10.1016/j.still.2019.104293.

Keller, T., Or, D., 2022. Farm vehicles approaching weights of sauropods exceed safe mechanical limits for soil functioning. Proc. Natl. Acad. Sci. 119 (21), e2117699119. https://doi.org/10.1073/pnas.2117699119.

Koorevaar, P., Menelik, G., Dirksen, C., 1983. Elements of Soil Physics. Elsevier.

Kozlowski, T.T., 1999. Soil compaction and growth of woody plants. Scand. J. For. Res. 14 (6), 596–619. https://doi.org/10.1080/02827589908540825.

Lawson, T., Blatt, M.R., 2014. Stomatal size, speed, and responsiveness impact on photosynthesis and water use efficiency. Plant Physiol. 164 (4), 1556–1570. https://doi.org/10.1104/pp.114.237107.

Lichtenthaler, H.K., 1987. Chlorophylls and carotenoids: pigments of photosynthetic biomembranes. Methods Enzymol. 148, 350–382. https://doi.org/10.1016/0076-6879(87)48036-1.

Lima, R.P., Rolim, M.M., Toledo, M.P., Tormena, C.A., da Silva, A.R., Silva, I.A.C., Pedrosa, E.M., 2022. Texture and degree of compactness effect on the pore size distribution in weathered tropical soils. Soil Tillage Res. 215, 105215. https://doi.org/10.1016/j.still.2021.105215.

Liu, J., Van Iersel, M.W., 2021. Photosynthetic physiology of blue, green, and red light: light intensity effects and underlying mechanisms. Front. Plant Sci. 12, 328. https://doi.org/10.3389/fpls.2021.619987.

Malavolta, E.A., Vitti, G.C., Oliveira, S.A., 1997. Avaliação do estado nutricional das plantas: princípios e aplicações. Piracicaba, Potafos. 201p.

Mariotti, B., Hoshika, Y., Cambi, M., Marra, E., Feng, Z., Paoletti, E., Marchi, E., 2020. Vehicle-induced compaction of forest soil affects plant morphological and physiological attributes: a meta-analysis. For. Ecol. Manag. 462, 118004. https://doi.org/10.1016/j.foreco.2020.118004.

Masle, J., Passioura, J.B., 1987. The effect of soil strength on the growth of young wheat plants. Funct. Plant Biol. 14 (6), 643–656.

McGarry, D., 1990. Soil compaction and cotton growth on a Vertisol. Soil Res. 28 (6), 869–877. https://doi.org/10.1071/SR9900869.

McGarry, D., 1995. The optimisation of soil structure for cotton production. Challeng. Future: Proceed. World Cotton Res. Confer. 1, 169–176.

Merten, G.H., Minella, J.P.G., 2013. The expansion of Brazilian agriculture: soil erosion scenarios. Int. Soil Water Conserv. Res. 1, 37–48. https://doi.org/10.1016/S2095-6339(15)30029-0.

Miao, Y., Wang, X., Gao, L.H., Chen, Q.Y., Qu, M., 2016. Blue light is more essential than red light for maintaining the activities of photosystem II and I and photosynthetic electron transport capacity in cucumber leaves. J. Integr. Agric. 15, 87–100. https://doi.org/10.1016/S2095-3119(15)61202-3.

Niinemets, Ü., 2023. Variation in leaf photosynthetic capacity within plant canopies: optimization, structural, and physiological constraints and inefficiencies. Photosynth. Res. 158 (2), 131–149. https://doi.org/10.1007/s11120-023-01043-9.

Nouri, A., Lee, J., Yin, X., Tyler, D.D., Saxton, A.M., 2019. Thirty-four years of no-tillage and cover crops improve soil quality and increase cotton yield in Alfisols, Southeastern USA. Geoderma 337 (9), 98–1008. https://doi.org/10.1016/j.geoderma.2018.10.016.

Pinelli, P., Loreto, F., 2003. $^{12}CO_2$ emission from different metabolic pathways measured in illuminated and darkened C3 and C4 leaves at low, atmospheric and elevated CO2 concentration. J. Exp. Bot. 54, 1761–1769. https://doi.org/10.1093/jxb/erg187.

Reynolds, W.D., Bowman, B.T., Drury, C.F., Tan, C.S., Lu, X., 2002. Indicators of good soil physical quality: density and storage parameters. Geoderma 110, 131–146. https://doi.org/10.1016/S0016-7061(02)00228-8.

Pragg, B., Deepagoda, T.C., Cameron, K., Di, H., Clough, T.J., Carrick, S., 2024. Irrigation scheduling needs to consider both plant-available water and soil aeration requirements. Vadose Zone J 23 (4), e20344. https://doi.org/10.1002/vzj2.20344.

Reynolds, E.S., 1963. The use of lead citrate at high pH as an electron-opaque stain in electron microscopy. J. Cell Biol. 17, 208–212.

Rivera, M., Polanía, J., Ricaurte, J., Borrero, G., Beebe, S., Rao, I., 2019. Soil compaction induced changes in morpho-physiological characteristics of common bean. J. Soil Sci. Plant Nutr. 19, 217–227. https://doi.org/10.1007/s42729-019-0007-y.

Ronchi, C.P., DaMatta, F.M., Batista, K.D., Moraes, G.A., Loureiro, M.E., Ducatti, C., 2006. Growth and photosynthetic down-regulation in Coffea arabica in response to restricted root volume. Funct. Plant Biol. 33 (11), 1013–1023. https://doi.org/10.1071/fp06147.

Samborska, I.A., Kalaji, H.M., Sieczko, L., Borucki, W., Mazur, R., Kouzmanova, M., Goltsev, V., 2019. Can just one-second measurement of chlorophyll a fluorescence be used to predict sulfur deficiency in radish (Raphanus sativus L. sativus) plants? Current Plant Biol. 19, 100096. https://doi.org/10.1016/j.cpb.2018.12.002.

Savage, M.J., Ritchie, J.T., Bland, W.L., Dugas, W.A., 1996. Lower limit of soil water availability. Agron. J. 88, 844–851. https://doi.org/10.2134/agronj1996.00021962008800040024x.

Schjonning, P., van den Akker, J.J., Keller, T., Greve, M.H., Lamandé, M., Simojoki, A., Breuning-Madsen, H., 2015. Driver-pressure-state-impact-response (DPSIR) analysis and risk assessment for soil compaction—a European perspective. Adv. Agron. 133, 183–237. https://doi.org/10.1016/bs.agron.2015.06.001.

Shaheb, M.R., Venkatesh, R., Shearer, S.A., 2021. A review on the effect of soil compaction and is management for sustainable crop production. J. Biosyst. Eng. 46, 417–439. https://doi.org/10.1007/s42853-021-00117-7.

Sharkey, T.D., 2016. What gas exchange data can tell us about photosynthesis. Plant Cell Environ. 39, 1161–1163. https://doi.org/10.1111/pce.12641.

Shikanai, T., 2014. Central role of cyclic electron transport around photosystem I in the regulation of photosynthesis. Curr. Opin. Biotechnol. 26, 25–30. https://doi.org/10.1016/j.copbio.2013.08.012.

Shikanai, T., Yamamoto, H., 2017. Contribution of Cyclic and Pseudocyclic electron transport to the Formation of Proton motive force in chloroplasts. Mol. Plant 10, 20–29. https://doi.org/10.1016/j.molp.2016.08.004.

Silva, P.L.F., Tormena, C.A., Echer, F.R., Cagna, C.P., Rocha, C.H., Lima, R.P., 2024. Cover crops influence the physical hydric quality of a tropical sandy soil under no-tillage cotton cropping. Rev. Bras. Ciência do Solo 48, e0240026. https://doi.org/10.36783/18069657rbcs20240026.

Sitko, K., Rusinowski, S., Kalaji, H.M., Szopiński, M., Małkowski, E., 2017. Photosynthetic efficiency as bioindicator of environmental pressure in A. halleri. Plant Physiol. 175, 290–302. https://doi.org/10.1104/pp.17.00212.

Strasser, R.J., Srivastava, A., Tsimilli-Michael, M., 2000. The fluorescence transient as a tool to characterise and screen photosynthetic samples. Probi. Photosynthesis: Mech. Regul. Adapt. 443–480.

Toshoji, H., Katsumata, T., Takusagawa, M., Yusa, Y., Sakai, A., 2012. Effects of chloroplast dysfunction on mitochondria: white sectors in variegated leaves have higher mitochondrial DNA levels and lower dark respiration rates than green sectors. Protoplasma 249, 805–817. https://doi.org/10.1007/s00709-011-0325-y.

Trethewey, R.N., Geigenberger, P., Riedel, K., Hajirezaei, M.R., Sonnewald, U., Stitt, M., Willmitzer, L., 1998. Combined expression of glucokinase and invertase in potato tubers leads to a dramatic reduction in starch accumulation and a stimulation of glycolysis. Plant J. 15 (1), 109–118. https://doi.org/10.1046/j.1365-313x.1998.00190.x.

Wieniarska, J., Lipecki, J., Stanek, R., Kesik, T., 1987. The effects of soil compaction due to machinery operation on a raspberry plantation. Fruit Sci. Rep. (Skierniewice) 14 (2).

Wolfe, D.W., Topoleski, D.T., Gundersheim, N.A., Ingall, B.A., 1995. Growth and yield sensitivity of four vegetable crops to soil compaction. J. Am. Soc. Hortic. Sci. 120 (6), 956–963.

Zar, J.H., 2010. Biostatistical Analysis, fifth ed. Prentice-Hall/Pearson, Upper Saddle River, xiii, p. 944.

Zelitch, I., Schultes, N.P., Peterson, R.B., Brown, P., Brutnell, T.P., 2009. High glycolate oxidase activity is required for survival of maize in normal air. Plant Physiol. 149 (1), 195–204. https://doi.org/10.1104/pp.108.128439.

Zhang, T., Folta, K.M., 2012. Green light signaling and adaptive response. Plant Signal. Behav. 7 (1), 75–78. https://doi.org/10.4161/psb.7.1.18635.

Zhen, S., Bugbee, B., 2020. Far-red photons have equivalent efficiency to traditional photosynthetic photons: implications for redefining photosynthetically active radiation. Plant Cell Environ. 43 (5), 1259–1272. https://doi.org/10.1111/pce.13730.